Table 1. Transcription-related genes highly expressed in E11.5 NPCs

Probe set ID	GenBank ID	Gene symbol	E11.5 NPCs	E14.5 NPCs	E11.5/ E14.5
1433919_at	AV302111	*Asb4*	9.8	0.5	19.6
1419406_a_at	NM_016707	***Bcl11a***	13.8	1.8	7.7
1418271_at	NM_021560	***Bhlhb5***	10.6	1.2	8.8
1452207_at	Y15163	*Cited2*	16.7	2.6	6.4
1449470_at	NM_010053	*Dlx1*	13.8	2.4	5.8
1448877_at	NM_010054	*Dlx2*	9.8	1.8	5.4
1449863_a_at	NM_010056	*Dlx5*	11.2	0.7	16.0
1459211_at	AW546128	*Gli2*	8.0	1.5	5.3
1456067_at	AW546010	*Gli3*	20.6	2.1	9.8
1422851_at	X58380	***Hmga2***	25.5	0.5	51.0
1450723_at	BQ176915	*Isl1*	8.6	0.1	86.0
1427300_at	D49658	*Lhx8*	10.5	0.1	105.0
1417155_at	BC005453	***N-myc***	8.2	1.2	6.8
1415811_at	BB702754	*NP95*	12.6	2.1	6.0
1421193_a_at	NM_016768	*Pbx3*	12.3	1.6	7.7
1417400_at	NM_030690	*Rai14*	11.0	1.6	6.9
1435856_x_at	AV310148	*Smarcb1*	8.0	1.6	5.0
1431255_at	BB656631	***Sox11***	38.7	6.2	6.2
1450034_at	AW214029	*Stat1*	9.6	1.8	5.3
1416711_at	NM_009322	*Tbr1*	9.8	0.2	49.0
1423424_at	BB732077	*Zic3*	11.2	0.5	22.4

Genes reported to participate in cell growth, differentiation and chromatin remodeling are shown in boldface.

Spatio-temporal expression patterns of genes highly expressed in E11.5 NPCs

To substantiate the GeneChip results, we extracted RNA from E11.5 and E14.5 NPCs and performed real-time RT-PCR using specific primers for each selected gene. Consistent with the GeneChip analysis, all five genes were highly expressed in E11.5 NPCs compared with E14.5 NPCs (Fig. 2A). We next performed *in situ* hybridization for each gene using E11.5, E14.5 and E17.5 mouse brain sections (Fig. 2B). *N-myc* and *Hmga2* mRNAs were specifically detected in the ventricular zone (VZ) of E11.5 brain, implying that N-myc and Hmga2 play some role in NPCs at this stage. By contrast, *Bhlhb5*, *Sox11* and *Bcl11a* expression was stronger in cortical plate, where postmitotic neurons reside, than in the VZ (Fig. 2B). We therefore decided to analyze the function of N-myc and Hmga2 in more detail.

Transduction of *N-myc* and *Hmga2* inhibits astrocyte differentiation of E14.5 NPCs

We next examined whether N-myc and Hmga2 affect astrocyte differentiation of NPCs. We expressed EGFP alone (control), and EGFP together with either N-myc or Hmga2, using retroviral infection in E14.5 NPCs, in which expression of the endogenous genes is very low. Virus-infected E14.5 NPCs were cultured for 4 days in the presence of LIF to induce astrocyte differentiation, and then stained with antibodies against GFP and GFAP. As shown in Fig. 3A and B, NPCs infected with control virus effectively differentiated into GFAP-positive astrocytes in response to LIF stimulation (42±2.6%). In contrast, GFAP-positive astrocyte differentiation was virtually abolished in cells ectopically expressing N-myc (0.5±0.4%) and Hmga2 (3±2.0%) (Fig. 3A, B). Expression of these genes did not significantly affect neuronal differentiation of NPCs, as assessed by monitoring expression of the neuronal marker βIII-tubulin, compared with the control cells (Fig. 3C, D). We further examined whether the observed suppression of astrocyte differentiation of NPCs infected with viruses encoding N-myc or Hmga2 could be attributed to specific cell-growth inhibition or to cell death. To address this issue, we performed immune staining for the cycling cell marker Ki67 and the apoptotic marker cleaved caspase 3. Although proliferation of NPCs ectopically expressing N-myc or Hmga2 appeared to be slightly enhanced, expression of either gene caused negligible cell death. These results suggest that N-myc and Hmga2 inhibit astrocyte differentiation of NPCs by a mechanism distinct from that of the neurogenic bHLH factors, which enhance neuronal differentiation (Sun et al., 2001).

Continuous expression of N-myc and Hmga2 in E11.5 NPCs fails to preserve the hypermethylated status of an astrocyte-specific gene promoter

We have previously shown that the *gfap* promoter is highly methylated in E11.5 NPCs, and becomes demethylated as gestation proceeds (Takizawa et al., 2001). This demethylation enables NPCs at later developmental stages, E14.5 or thereafter, to respond to LIF and differentiate into GFAP-positive astrocytes. As shown in the foregoing data, expression levels of *N-myc* and *Hmga2* thus seemed to be reduced concurrently with the developmental stage-dependent demethylation of an astrocyte-specific gene promoter; furthermore, ectopic expression of these genes in E14.5 NPCs inhibited GFAP-positive astrocyte differentiation. We therefore hypothesized that sustained expression of N-myc and Hmga2 in E11.5 NPCs might maintain the hypermethylated status of the *gfap* promoter. To test this, we infected E11.5 NPCs with viruses expressing EGFP alone and EGFP together with either N-myc or Hmga2 and cultured them for 4 days. GFP-positive cells were sorted by FACS and their genomic DNAs were extracted for bisulfite sequencing. As observed in the previous study (Takizawa et al., 2001), the *gfap* promoter including the STAT3 site became demethylated to about 65% in control virus-infected cells after the 4-day culture, and this was also the case for both N-myc- and Hmga2-expressing virus-infected cells (Fig. 3E, F). These results indicate that sustained expression of N-myc and Hmga2 in E11.5 NPCs does not affect the process of demethylation in this astrocyte-specific gene promoter. On the other hand, when 4-day-cultured control virus-infected E11.5 NPCs were then stimulated with LIF for an additional 4 days, GFAP-positive astrocytes appeared, probably due to demethylation in the promoter, whereas neither *N-myc* nor *Hmga2* virus-infected cells gave rise to astrocytes even in the presence of LIF (data not shown). These results suggest that N-myc and Hmga2 inhibit precocious astrocyte differentiation of midgestational NPCs independent of the DNA methylation status of an astrocyte-specific gene promoter.

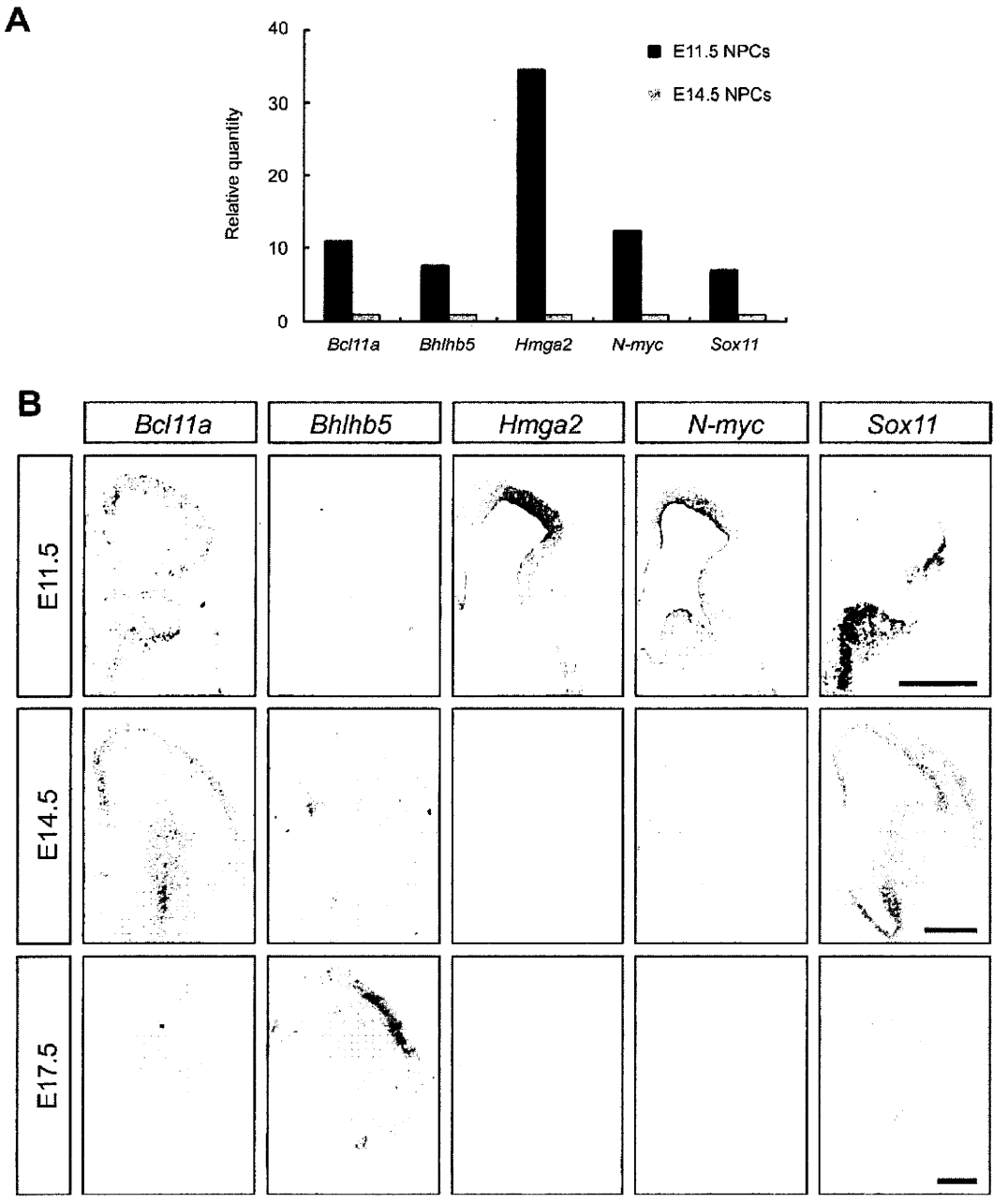

Fig. 2. *N-myc* and *Hmga2* are highly expressed in the VZ of E11.5 mouse brain. (A) Gene-specific real-time RT-PCR was performed to validate GeneChip analysis data. (B) *In situ* hybridization was performed for E11.5, E14.5 and E17.5 mouse brain sections. No signal was detected when sense-probes for each gene were used (data not shown). Scale bar=500 μm.

DISCUSSION

In this study, we compared NPC gene expression profiles at different developmental stages using Affymetrix GeneChips and the Percellome method, and then analyzed by *in situ* hybridization the spatio-temporal expression patterns of genes which were highly expressed in E11.5 NPCs. We found that *N-myc* and *Hmga2* were specifically expressed in E11.5 NPC both *in vivo* and *in vitro* and, furthermore, that the transduction of these genes into NPCs suppressed LIF-induced astrocytic differentiation without affecting DNA demethylation of the astrocyte-specific *gfap* gene promoter.

The basic HLH leucine zipper transcription factor N-myc,a member of the myc family of oncogenes, is a nuclear phosphoprotein exhibiting site-specific DNA-binding activity (Ramsay et al., 1986; Alex et al., 1992), and has

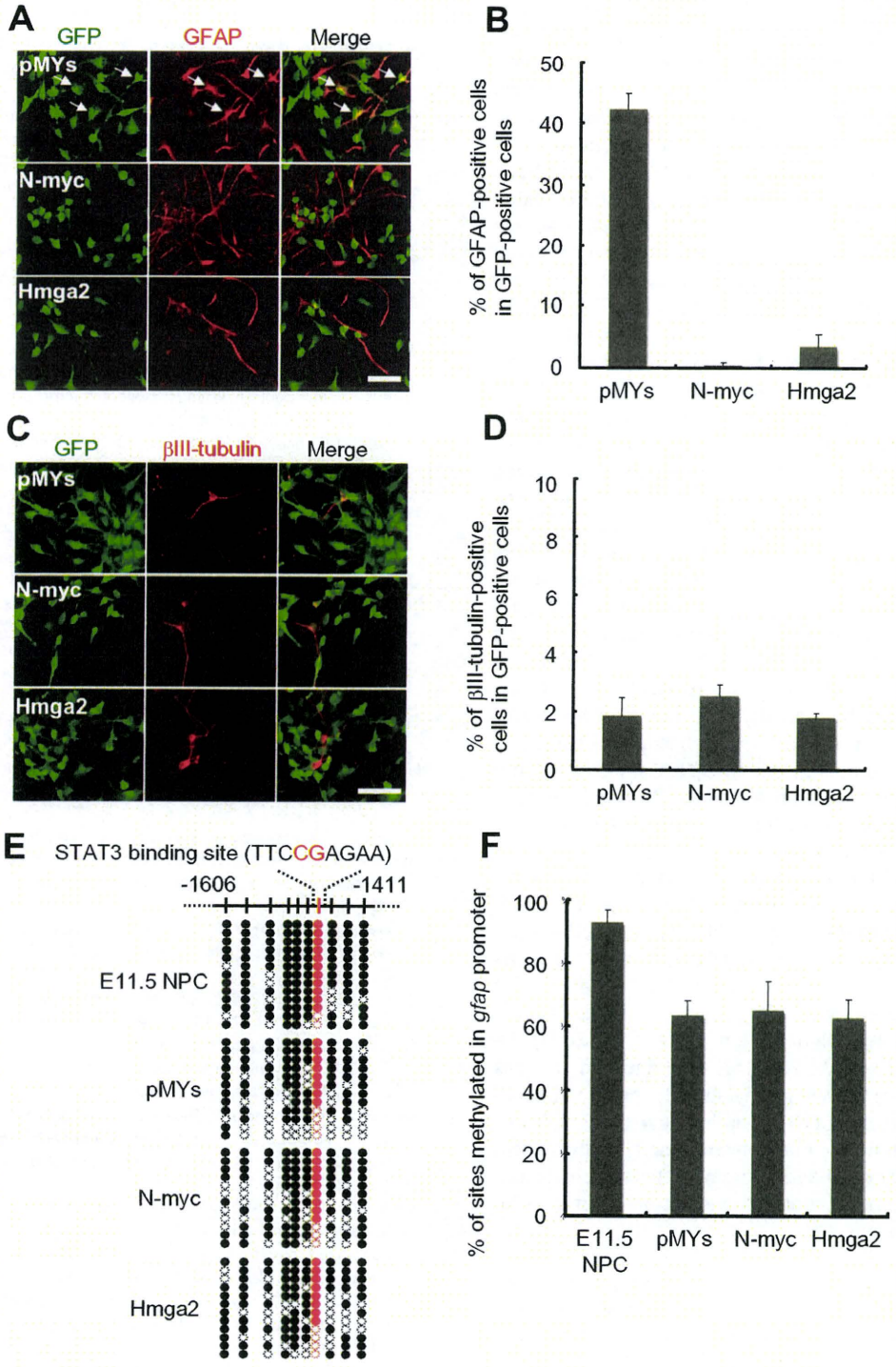

Fig. 3. N-myc and Hmga2 inhibit astrocyte differentiation of NPCs even in the presence of LIF. (A–D) E14.5 NPCs were infected with recombinant retroviruses engineered to express *EGFP* alone (pMYs), and *EGFP* together with either *N-myc* (N-myc) or *Hmga2* (Hmga2), and cultured with LIF (50 ng/ml) for 4 days to induce astrocyte differentiation. The cells were then stained with antibodies against GFP (green) and GFAP (red) (A). Arrows indicate GFP/GFAP double-positive cells. The percentage of GFAP-positive astrocytes in GFP-positive cells was quantified (B). Mean±S.D. The cells were also stained with antibodies against GFP (green) and βIII-tubulin (red) (C). The percentage of βIII-tubulin-positive neurons in GFP-positive cells was quantified (D). Mean±S.D. (E) E11.5 NPCs were infected with recombinant retroviruses engineered to express *EGFP* alone (pMYs), and *EGFP* together with either *N-myc* (N-myc) or *Hmga2* (Hmga2), and subsequently cultured for 4 days. GFP-positive cells were then sorted based on GFP fluorescence, and genomic DNA was extracted for bisulfite sequencing. White and black circles indicate unmethylated and methylated CpG sites, respectively. The E11.5 NPC sample was freshly prepared NPCs from telencephalon at E11.5. The CpG dinucleotide within the STAT3 binding site is indicated in red. (F) Methylation frequency in the *gfap* promoter. Mean±S.D. Scale bars=50 μm (A, C). For interpretation of the references to color in this figure legend, the reader is referred to the Web version of this article.

been reported to be expressed in a wide range of vertebrate tissues, primarily during embryogenesis (Schreiber-Agus et al., 1993). The mice deficient for functional *N-myc* are embryonic lethal (Stanton et al., 1992). Since N-myc has been shown to be a transcriptional activator, it may inhibit astrocyte differentiation via induction of neurogenic bHLH factors such as *Ngn1* (Sun et al., 2001), which have already been suggested to inhibit astrocyte differentiation in midgestational NPCs. However, this scenario seems unlikely because *N-myc* expression in NPCs did not affect neuronal differentiation, as assessed by monitoring expression of the neuronal marker βIII-tubulin (Fig. 3C, D). On the other hand, Hmga2 possesses an acidic C-terminal tail and three individual DNA-binding domains which bind short stretches of AT-rich DNA with high affinity (Reeves, 2001). *Hmga2* is expressed in pluripotent embryonic stem (ES) cells and in most tissues and organs during embryogenesis, but at very low levels or not at all in adult tissues (Zhou et al., 1995). Its function appears to be critical for cell growth, because mice lacking functional *Hmga2* exhibit a pygmy phenotype (Zhou et al., 1995). Recently, it was reported that Hmga2 specifically accumulates on senescent cell chromatin and that it functions as a structural component of senescence-associated heterochromatin foci and as a repressor of proliferation-associated genes (Narita et al., 2006). We therefore expected that Hmga2 would maintain the hypermethylation status of the astrocyte-specific *gfap* promoter via transcription-repressive heterochromatin formation in E11.5 NPCs. However, our results indicate that this is not the case. The mechanism(s) whereby N-myc and Hmga2 inhibit astrocyte differentiation must await further investigation.

Although DNA methylation is a critical cell-intrinsic determinant for the neurogenic-to-astrogliogenic switch and/or astrocyte differentiation of NPCs, many other spatio-temporally expressed extracellular factors such as CT-1, Notch and Wnt1 (Barnabe-Heider et al., 2005; Hirabayashi and Gotoh, 2005; Nagao et al., 2007) and intracellular factors including Ngn (Sun et al., 2001), N-CoR (Hermanson et al., 2002), N-myc and Hmga2 (this study) complement DNA methylation to ensure the sequential differentiation of NPCs during development. Thus, to better understand the mechanism underlying these processes, this study emphasizes the need to take cell-extrinsic cues, cell-intrinsic programs and factors, and their interaction into consideration.

Acknowledgments—We thank Dr. T. Kitamura (Tokyo University) for pMY vector and Plat-E cells. We appreciate Dr. Y. Bessho and T. Matsui for valuable discussions. We also thank Dr. I. Smith for helpful comments and critical reading of the manuscript. We are very grateful to N. Ueda for excellent secretarial assistance. Many thanks to N. Namihira for technical help. We also thank N. Moriyama for technical help with GeneChip analysis. This work has been supported by a Grant-in-Aid for Science Research on Priority Areas and the NAIST Global COE Program (Frontier Biosciences: Strategies for survival and adaptation in a changing global environment) from the Ministry of Education, Culture, Sports, Science and Technology (MEXT) of Japan.

REFERENCES

Abramova N, Charniga C, Goderie SK, Temple S (2005) Stage-specific changes in gene expression in acutely isolated mouse CNS progenitor cells. Dev Biol 283:269–281.

Ajioka I, Maeda T, Nakajima K (2006) Identification of ventricular-side-enriched molecules regulated in a stage-dependent manner during cerebral cortical development. Eur J Neurosci 23:296–308.

Alex R, Sozeri O, Meyer S, Dildrop R (1992) Determination of the DNA sequence recognized by the bHLH-zip domain of the N-Myc protein. Nucleic Acids Res 20:2257–2263.

Barnabe-Heider F, Wasylnka JA, Fernandes KJ, Porsche C, Sendtner M, Kaplan DR, Miller FD (2005) Evidence that embryonic neurons regulate the onset of cortical gliogenesis via cardiotrophin-1. Neuron 48:253–265.

Bonni A, Sun Y, Nadal-Vicens M, Bhatt A, Frank DA, Rozovsky I, Stahl N, Yancopoulos GD, Greenberg ME (1997) Regulation of gliogenesis in the central nervous system by the JAK-STAT signaling pathway. Science 278:477–483.

Brunelli S, Innocenzi A, Cossu G (2003) Bhlhb5 is expressed in the CNS and sensory organs during mouse embryonic development. Gene Expr Patterns 3:755–759.

Bugga L, Gadient RA, Kwan K, Stewart CL, Patterson PH (1998) Analysis of neuronal and glial phenotypes in brains of mice deficient in leukemia inhibitory factor. J Neurobiol 36:509–524.

Cai L, Morrow EM, Cepko CL (2000) Misexpression of basic helix-loop-helix genes in the murine cerebral cortex affects cell fate choices and neuronal survival. Development 127:3021–3030.

Edlund T, Jessell TM (1999) Progression from extrinsic to intrinsic signaling in cell fate specification: a view from the nervous system. Cell 96:211–224.

Graham V, Khudyakov J, Ellis P, Pevny L (2003) SOX2 functions to maintain neural progenitor identity. Neuron 39:749–765.

He F, Ge W, Martinowich K, Becker-Catania S, Coskun V, Zhu W, Wu H, Castro D, Guillemot F, Fan G, de Vellis J, Sun YE (2005) A positive autoregulatory loop of Jak-STAT signaling controls the onset of astrogliogenesis. Nat Neurosci 8:616–625.

Hermanson O, Jepsen K, Rosenfeld MG (2002) N-CoR controls differentiation of neural stem cells into astrocytes. Nature 419: 934–939.

Hirabayashi Y, Gotoh Y (2005) Stage-dependent fate determination of neural precursor cells in mouse forebrain. Neurosci Res 51: 331–336.

Hsieh J, Gage FH (2004) Epigenetic control of neural stem cell fate. Curr Opin Genet Dev 14:461–469.

Kanno J, Aisaki K, Igarashi K, Nakatsu N, Ono A, Kodama Y, Nagao T (2006) "Per cell" normalization method for mRNA measurement by quantitative PCR and microarrays. BMC Genomics 7:64.

Knoepfler PS, Cheng PF, Eisenman RN (2002) N-myc is essential during neurogenesis for the rapid expansion of progenitor cell populations and the inhibition of neuronal differentiation. Genes Dev 16:2699–2712.

Koblar SA, Turnley AM, Classon BJ, Reid KL, Ware CB, Cheema SS, Murphy M, Bartlett PF (1998) Neural precursor differentiation into astrocytes requires signaling through the leukemia inhibitory factor receptor. Proc Natl Acad Sci U S A 95:3178–3181.

Morita S, Kojima T, Kitamura T (2000) Plat-E: an efficient and stable system for transient packaging of retroviruses. Gene Ther 7: 1063–1066.

Nagao M, Sugimori M, Nakafuku M (2007) Cross talk between notch and growth factor/cytokine signaling pathways in neural stem cells. Mol Cell Biol 27:3982–3994.

Nakashima K, Wiese S, Yanagisawa M, Arakawa H, Kimura N, Hisatsune T, Yoshida K, Kishimoto T, Sendtner M, Taga T (1999a) Developmental requirement of gp130 signaling in neuronal survival and astrocyte differentiation. J Neurosci 19:5429–5434.

Nakashima K, Yanagisawa M, Arakawa H, Kimura N, Hisatsune T, Kawabata M, Miyazono K, Taga T (1999b) Synergistic signaling in

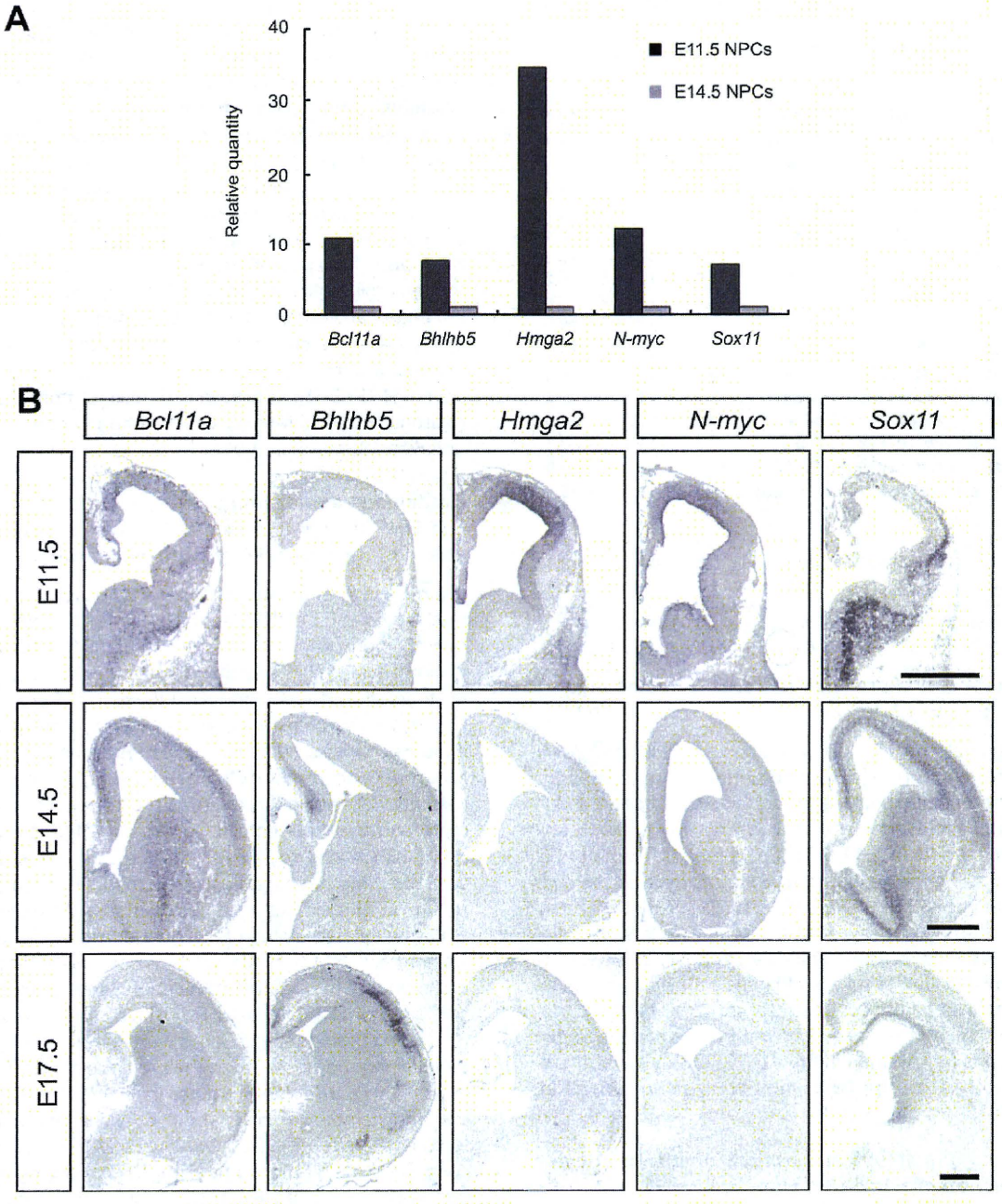

Fig. 2. *N-myc* and *Hmga2* are highly expressed in the VZ of E11.5 mouse brain. (A) Gene-specific real-time RT-PCR was performed to validate GeneChip analysis data. (B) *In situ* hybridization was performed for E11.5, E14.5 and E17.5 mouse brain sections. No signal was detected when sense-probes for each gene were used (data not shown). Scale bar=500 μm.

DISCUSSION

In this study, we compared NPC gene expression profiles at different developmental stages using Affymetrix GeneChips and the Percellome method, and then analyzed by *in situ* hybridization the spatio-temporal expression patterns of genes which were highly expressed in E11.5 NPCs. We found that *N-myc* and *Hmga2* were specifically expressed in E11.5 NPC both *in vivo* and *in vitro* and, furthermore, that the transduction of these genes into NPCs suppressed LIF-induced astrocytic differentiation without affecting DNA demethylation of the astrocyte-specific *gfap* gene promoter.

The basic HLH leucine zipper transcription factor N-myc,a member of the myc family of oncogenes, is a nuclear phosphoprotein exhibiting site-specific DNA-binding activity (Ramsay et al., 1986; Alex et al., 1992), and has

OPEN ACCESS Freely available online

PLoS one

Astrocyte-Specific Genes Are Generally Demethylated in Neural Precursor Cells Prior to Astrocytic Differentiation

Izuho Hatada[1]*, Masakazu Namihira[2], Sumiyo Morita[1], Mika Kimura[1], Takuro Horii[1], Kinichi Nakashima[2]

1 Laboratory of Genome Science, Biosignal Genome Resource Center, Institute for Molecular and Cellular Regulation, Gunma University, Maebashi, Japan, **2** Laboratory of Molecular Neuroscience, Graduate School of Biological Sciences, Nara Institute of Science and Technology, Ikoma, Japan

Abstract

Epigenetic changes are thought to lead to alterations in the property of cells, such as differentiation potential. Neural precursor cells (NPCs) differentiate only into neurons in the midgestational brain, yet they become able to generate astrocytes in the late stage of development. This differentiation-potential switch could be explained by epigenetic changes, since the promoters of astrocyte-specific marker genes, glial fibrillary acidic protein (*Gfap*) and *S100β*, have been shown to become demethylated in late-stage NPCs prior to the onset of astrocyte differentiation; however, whether demethylation occurs generally in other astrocyctic genes remains unknown. Here we analyzed DNA methylation changes in mouse NPCs between the mid-(E11.5) and late (E14.5) stage of development by a genome-wide DNA methylation profiling method using microarrays and found that many astrocytic genes are demethylated in late-stage NPCs, enabling the cell to become competent to express these genes. Although these genes are already demethylated in late-stage NPCs, they are not expressed until cells differentiate into astrocytes. Thus, late-stage NPCs have epigenetic potential which can be realized in their expression after astrocyte differentiation.

Citation: Hatada I, Namihira M, Morita S, Kimura M, Horii T, et al. (2008) Astrocyte-Specific Genes Are Generally Demethylated in Neural Precursor Cells Prior to Astrocytic Differentiation. PLoS ONE 3(9): e3189. doi:10.1371/journal.pone.0003189

Editor: Peter Fraser, The Babraham Institute, United Kingdom

Received April 21, 2008; **Accepted** August 19, 2008; **Published** September 11, 2008

Copyright: © 2008 Hatada et al. This is an open-access article distributed under the terms of the Creative Commons Attribution License, which permits unrestricted use, distribution, and reproduction in any medium, provided the original author and source are credited.

Funding: This study was supported in part by grants from the Japanese Science and Technology Agency, the Ministry of Education, Culture, Sports, Science and Technology of Japan, and the Ministry of Health, Labor, and Welfare of Japan. The funders had no role in study design, data collection and analysis, decision to publish, or preparation of the manuscript.

Competing Interests: The authors have declared that no competing interests exist.

* E-mail: ihatada@showa.gunma-u.ac.jp

Introduction

DNA methylation usually occurs in mammalian cells at CpG dinucleotides and approximately 60–90% of cytosines at these sites are methylated [1]. Most CpG-rich DNA fragments, or CpG islands in genes, have been thought to remain unmethylated even in cell types that do not express the genes [2]. However, changes in DNA methylation have been sporadically observed in CpG islands during development and are thought to play important roles in the regulation of cell type-specific gene expression [3,4]. DNA methylation also participates in the regulation of differentiation and embryonic development [5]. For example, inactivation of *Oct3/4* (*Pou5f1*) and *Nanog* genes by DNA methylation is important for early development [6,7]. These genes are essential for maintaining pluripotency of embryonic stem (ES) cells and early embryos [8,9,10] and are also known as two of four genes which have been shown to reprogram somatic cells to pluripotent stem (iPS) cells with the essential characteristics of embryonic stem (ES) cells [11].

Epigenetic modification is also thought to play an important role in altering the differentiation potential of neural precursor cells (NPCs). NPCs differentiate only into neurons in the midgestational brain, while they become able to generate astrocytes as gestation proceeds [12]. The Janus kinase (JAK) signal transducer and activator of the transcription (STAT) pathway, which is activated by cytokines, including leukemia inhibitory factor (LIF), can effectively induce astrocyte differentiation [13,14]. A particular cytosine residue within a STAT3-binding site in the astrocyte-specific marker glial fibrillary acidic protein (*Gfap*) gene promoter is highly methylated in NPCs midgestation (E11.5) when astrogenesis does not normally occur, while it becomes demethylated in late-stage (E14.5) NPCs that are prone to differentiating into astrocytes [15]. Although these late-stage (E14.5) NPCs with demethylated promoter do not express *Gfap*, the expression can be upregulated upon differentiation by leukemia inhibitory factor (LIF), which induces STAT3-activating cytokines [13,14].

Previously, we developed a genome-wide DNA methylation analysis called Microarray-based Integrated Analysis of Methylation by Isoschizomers (MIAMI) using a microarray with genome-wide probes and used for several applications [16,17]. With this method, we detected DNA methylation using the methylation-sensitive restriction enzyme *Hpa* II and its methylation-insensitive isoschizomer *Msp* I.

Although the demethylation of *Gfap* is known in late-stage NPCs prior to astrocyte differentiation [15], it is not known whether other genes confer this astrocytic property to cells. To study the role of DNA methylation in altering the differentiation potential of NPCs, here we analyzed DNA methylation changes in mouse NPCs between the mid-(E11.5) and late (E14.5) stages of development by a genome-wide DNA methylation profiling method using microarrays. We also compared the methylation status with that of postnatal day 1 (P1) astrocytes.

Results and Discussion

Genome-wide profiling of DNA methylation

Methylation changes in the differentiation potential switch of NPCs were analyzed by comparing mid-(E11.5) and late (E14.5)-stage NPCs using the MIAMI method [16]. We also compared the

methylation status with that of postnatal day 1 (P1) astrocytes. Before analysis, the key genes involved in astrocyte differentiation, such as *Gfap* and *Stat3*, were analyzed for DNA methylation in the sample we used (Fig. 1). As described previously [15], the STAT3-binding site of *Gfap* gene was demethylated in E14.5 NPCs prior to astrocyte differentiation. On the other hand, the promoter of *Stat3* gene was unmethylated throughout differentiation. The microarray used consisted of probes chosen from the Agilent promoter array using an eArray system (http://earray.chem.agilent.com/earray/). The probes are located on *Hpa* II fragments of less than 1 kilobasepair (kb) and cover 14,543 genes. Probes which showed methylation changes at least in E14.5 NPCs or astrocytes compared to E11.5 NPCs are presented in Fig. 2A and Table S1 (Name of the probes and genes were indicated in Table S1). As shown in Fig. 2B, E14.5 NPCs are hypomethylated in 85 probes (80 genes) and hypermethylated in 15 probes (15 genes). On the other hand, astrocytes are hypomethylated in 275 probes (256 genes) and hypermethylated in 170 probes (152 genes). The reliability of the analysis was confirmed by bisulfite sequencing analysis of eight genes (Fig. 3). The methylation ratio analyzed by MIAMI (Fig. 3A) had good correlation with the methylation of two *Hpa* II sites adjacent to the probes (Fig. 3B). Interestingly 80% of the probes hypomethylated in E14.5 NPCs are also hypomethylated in astrocytes. (Fig. 2C). If we extend the hypomethylation change criteria to the threshold level (D10<0.5, usually we use D10<0.2 for hypomethylation), 89% of the probes hypomethylated in E14.5 NPCs are also hypomethylated in astrocytes. In other words, 48% of the hypomethylated probes in astrocytes are also hypomethylated in E14.5 NPCs. These include a probe for an astrocyte-specific marker gene, *Gfap*, which was previously shown to be hypomethylated both in E14.5 NPCs and astrocytes [15]. However, another hypomethylated astrocyte marker, S100β [18], was not detected by the MIAMI method because the DNA sequence with methylation change does not contain any *Hpa* II sites, leading to underestimation of the total number of genes actually demethylated in E14.5 NPCs. Nevertheless, including the genes undetectable by MIAMI, many hypomethylated sequences in astrocytes are already demethylated in E14.5 NPCs, which are competent to differentiate into astrocytes. These include important genes for astrocyte-specific function or phenotype in addition to an astrocyte-specific marker gene, *Gfap*. For example, Aldolase C encodes a member of the class I fructose-biphosphate aldolase gene family specific to astrocytes (*Aldoc*, 19). The demethylated region of *Aldoc* is located on exon 1. We further confirmed this result by bisulfite sequencing and found that *Aldoc* was methylated in E11.5 NPCs and demethylated in E14.5 NPCs and astrocytes (Fig. 3B). Another example, *Kcnj10* (*Kir4.1*), is widely expressed in astrocytes throughout the brain [20]. The product of this gene is absent in immature proliferating cells, and progressive expression of the genes correlates with astrocyte differentiation, which is characterized by the establishment of a negative membrane potential and exit from the cell cycle. *Kcnj10* (*Kir4.1*) encodes a member of the inward rectifier-type potassium channel family, characterized by having a greater tendency to allow potassium to flow into, rather than out of, a cell, resulting in negative membrane potential. The encoded protein is responsible for potassium buffering action, which is a major function of astrocytes and is also responsible for promoting differentiation and inhibiting cell growth [20,21]. Mutations in this gene have been associated with seizure susceptibility of common idiopathic generalized epilepsy syndromes [22,23]. *Sparcl1* is known as an astrocyte marker colocalized with *Gfap* [24] and is also known as a candidate gene for multiple sclerosis [25]. *Cbs* and *BC055107* are also known as astrocyte markers [26,27]. Thus, we found that demethylation

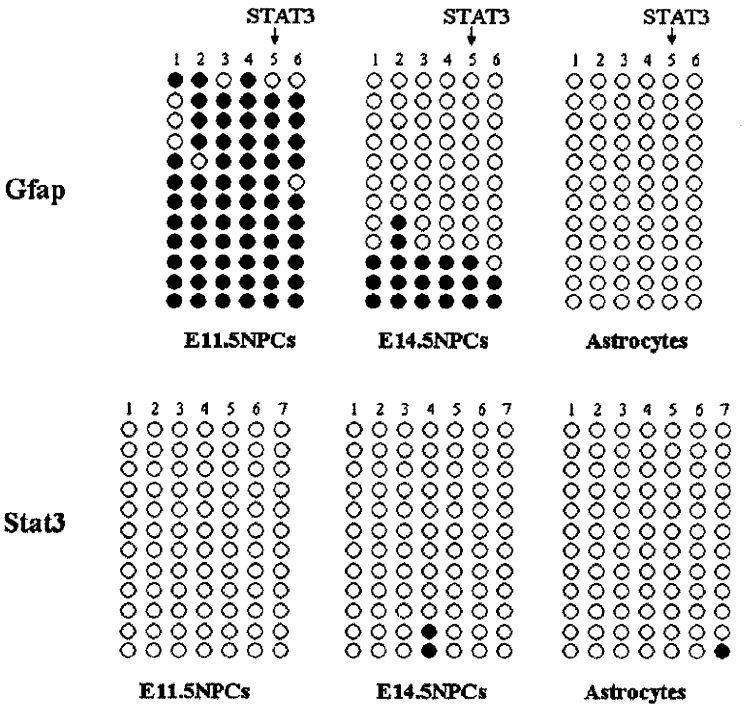

Figure 1. DNA methylation of *Gfap* and *Stat3* gene. DNA methylation was analyzed by bisulfite sequencing. Closed circles indicate methylated CpG sites and open circles indicate unmethylated CpG sites. STAT3 binding sites are indicated by arrows.
doi:10.1371/journal.pone.0003189.g001

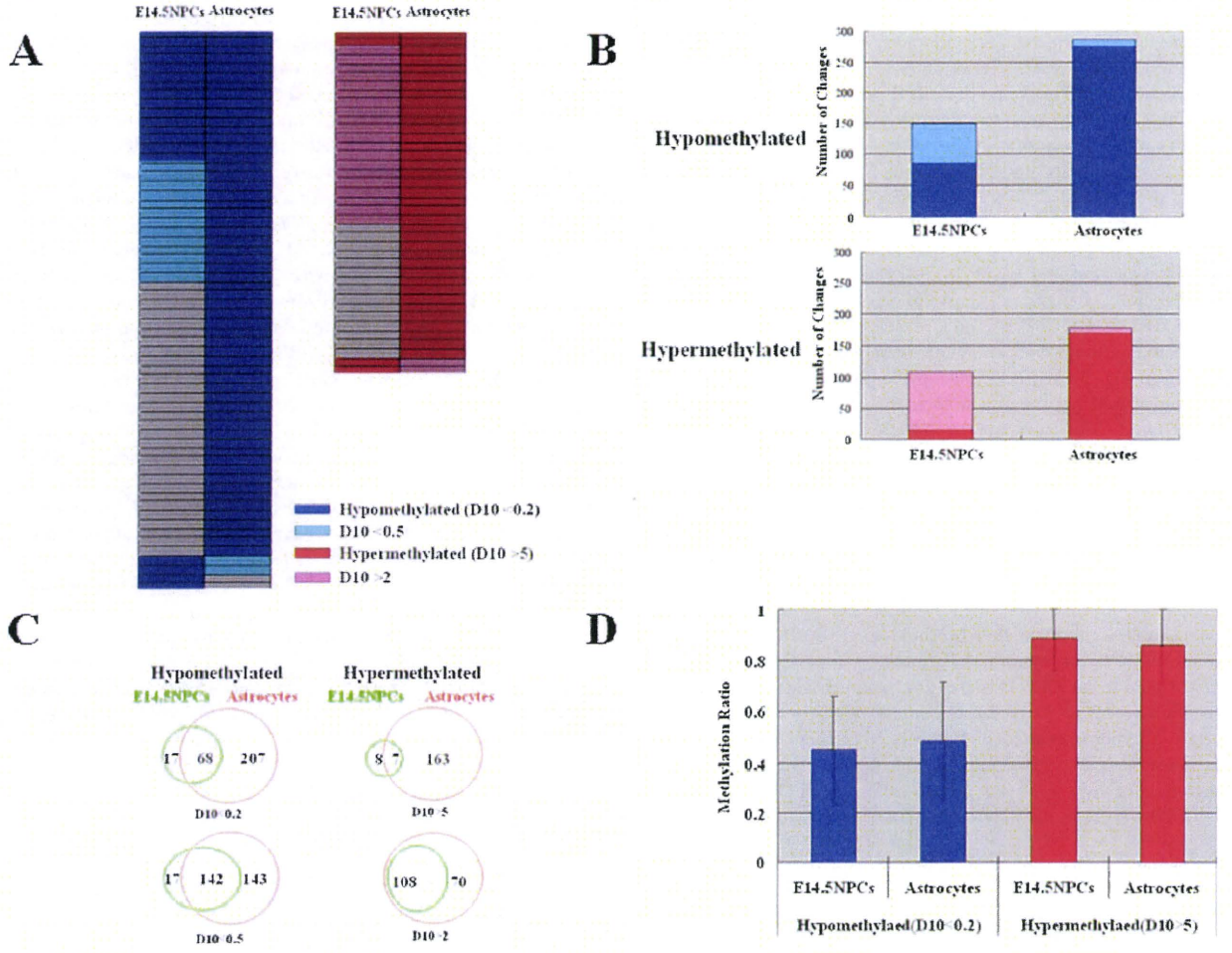

Figure 2. Genome-wide profiling of DNA methylation. (A) Hypomethylated and hypermethylated genes in E14.5 NPCs and astrocytes compared to E11.5 NPCs. Each row indicates each probe and each column indicates E14.5 NPCs or astrocytes. Probes with methylation changes are indicated in color. D10 is a value indicating the difference between methylation-sensitive *Hpa* II cleavage and methylation-insensitive *Msp* I cleavage. (B) Number of methylation changes in E14.5 NPCs and astrocytes compared to E11.5 NPCs. Numbers of methylation changes indicated in Fig. 1A were counted and indicated by bars. (C) Venn diagram of the number of probes with methylation changes in E14.5 NPCs and astrocytes compared to E11.5 NPCs. (D) Absolute levels of DNA methylation analyzed by MIAMI presented as methylation ratio. Methylation ratios of hypermethylated and hypomethylated probes are presented as average±standard deviation.
doi:10.1371/journal.pone.0003189.g002

occurred not only in *Gfap* but also in the other genes involved in astrogenesis prior to astrocyte differentiation.

When comparing methylation status between E14.5 NPCs and astrocytes, it is important to know what percentage of the E14.5 NPCs actually gives rise to astrocytes. After 4 day-culture in the presence of LIF, 30–40% of E14.5 NPCs become GFAP-positive, yet this does not necessary mean that *Gfap* promoter is methylated in all GFP-negative cells. We have previously shown that STAT site within the *Gfap* promoter was virtually unmethylated in E14.5 NPCs during 4-day culture in the proliferating condition. They, however, could not give rise to 100% of GFAP-positive cells [15]. These findings suggest the existence of other factors that inhibit astrocyte differentiation. Thus, it is conceivable that demethylation is necessary but not sufficient for NPCs to differentiate into GFAP-positive astrocytes.

Absolute levels of DNA methylation were analyzed by MIAMI and were presented as average methylation ratio for hypomethylated and hypermethylated genes compared to E11.5 NPCs (Fig. 2D). On average, hypermethylated genes were nearly fully methylated as expected. However, hypomethylated genes had some methylation on average. In addition, some hypomethylated genes, specially, *Aldoc* had highly mosaic pattern, suggesting a possibility that equilibrium state may have been reached rather than DNA demethylation (Fig. 3B).

A hallmark for Polycomb-mediated repression is methylation of lysine 27 histone H3 (H3K27), which is set up by the Polycomb repressive complex2 [28,29]. Many polycomb targets in embryonic stem cells (ESCs) have been shown to reside in a chromatin state characterized not only by the dual presence of repressive H3K27 methylation but also by active H3K4 methylation [30]. In neural differentiation, the promoters marked by H3K27 methylation in ESCs are more likely to become de novo DNA methylated [31]. Therefore, we analyzed the histone methylation status in ESCs for our hypermethylated genes in astrocytes compared to E11.5 NPCs using the published ESCs data [32]. We found that promoter that were marked by H3K27 in ESCs were significantly enriched in hypermethylated genes in astrocytes ($P<1\times10^{-14}$).

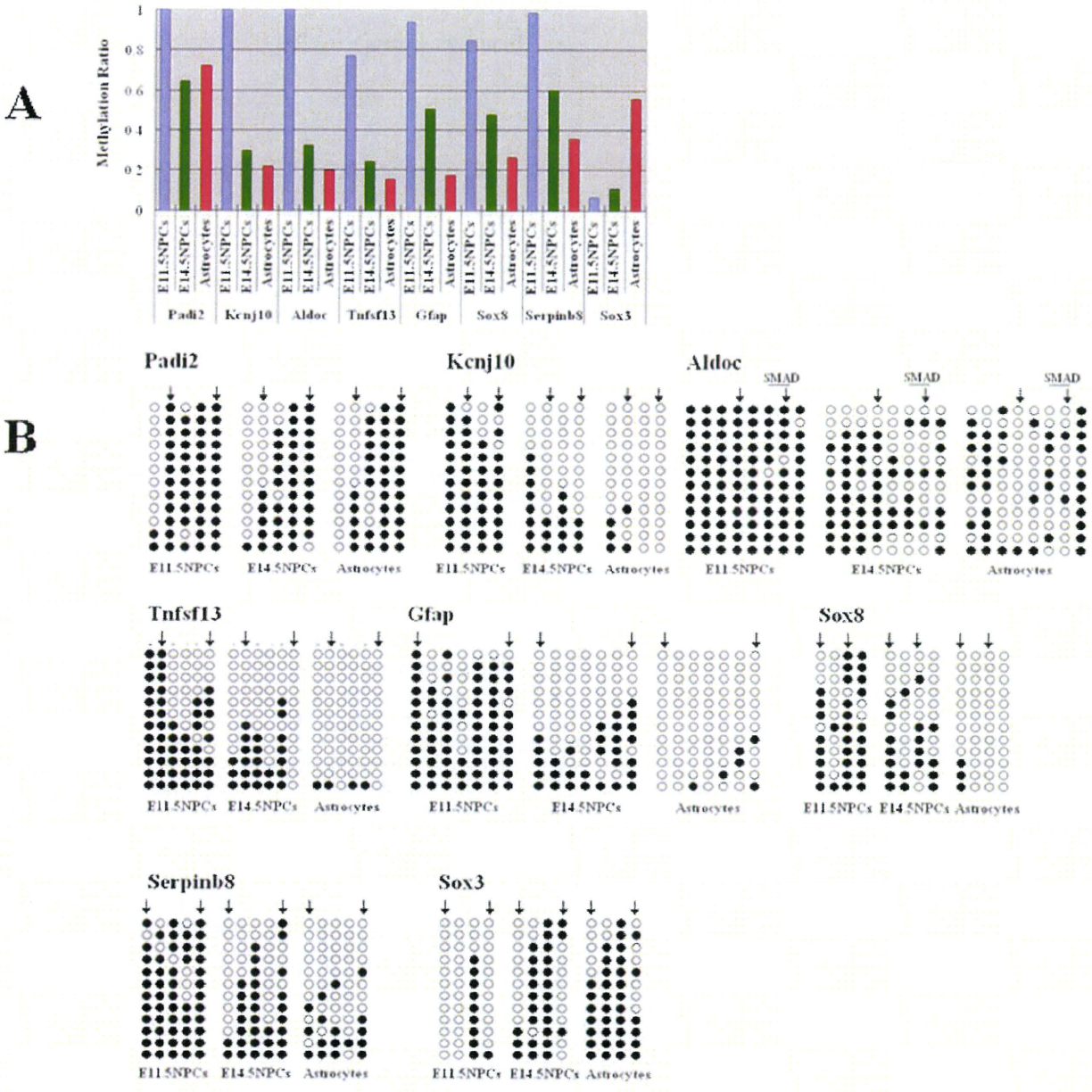

Figure 3. Confirmation of genome-wide methylation profiling by MIAMI. (A) Methylation ratios of seven hypomethylated and one hypermethylated gene compared to E11.5 NPCs. Methylation ratios are calculated by MIAMI data. (B) Confirmation of seven hypomethylated genes and one hypermethylated gene by bisulfite sequencing analysis. Closed circles indicate methylated CpG sites and open circles indicate unmethylated CpG sites. Positions of *Hpa* II sites are indicated as arrows.
doi:10.1371/journal.pone.0003189.g003

Expression changes in NPCs and astrocytes

Expression changes during the differentiation potential switch of NPCs were analyzed by comparing mid-(E11.5) and late (E14.5)-stage NPCs, and astrocytes by expression microarray analysis (Fig. 4, Table S2). We found that 49% of the probes upregulated in E14.5 NPCs compared to E11.5 NPCs were also upregulated in astroctyes (Fig. 3B). This is smaller than the ratio of hypomethylation where 80% of the probes hypomethylated in E14.5 NPCs were also hypothylated in astrocytes (Fig. 2C). This implies that astrocyte-specific genes, including *Gfap, Aldoc,* and *Kcnj10* (*Kir4.1*), are demethylated at E14.5 NPCs, while they are not expressed until cells differentiate into astrocytes. To examine this hypothesis, we analyzed the expression of genes hypomethylated both in E14.5 NPCs and astrocytes. Among these genes, those that showed upregulation in E14.5 NPCs or astrocytes compared to E11.5 NPCs are shown in Fig. 5. Of these, 64% of the genes, including astrocyte-specific marker *Gfap*, showed more than twice the expression level in astrocytes compared to E14.5 NPCs. Thus, genes already demethylated, such as *Gfap, Aldoc,* and *Kcnj10* (*Kir4.1*), were competent but not highly expressed in E14.5 NPCs,

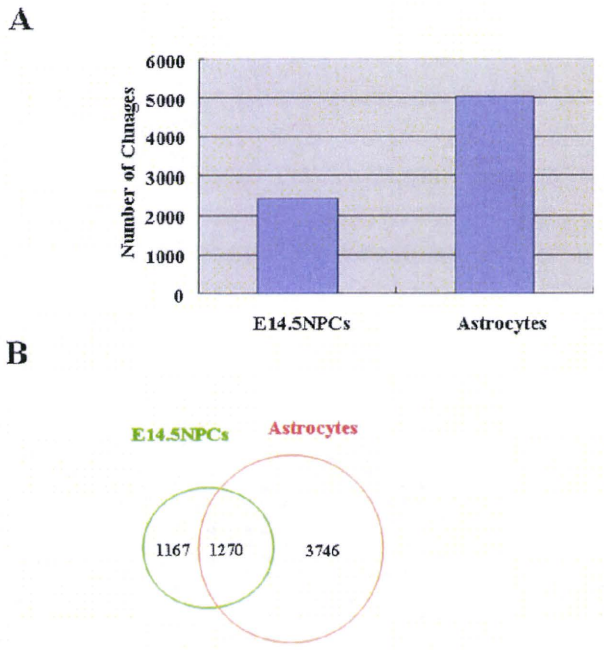

Figure 4. Expression analysis by microarray. (A) Number of upregulated genes in E14.5 NPCs and astrocytes compared to E11.5 NPCs. (B) Venn diagram of the number of upregulated genes in E14.5 NPCs and astrocytes compared to E11.5 NPCs.
doi:10.1371/journal.pone.0003189.g004

suggesting that their expression appears after differentiation into astrocytes (Fig. 6). Astrocyte-specific genes probably require the expression and/or activation of astrocyte-inducing transcription factors, such as STAT3, to be effectively expressed (Fig. 6).

To analyze the relation between the DNA methylation and the expression of genes, we plotted the methylation ratio calculated by MIAMI and the expression level calculated by expression microarray analysis for all genes examined (Fig. 7A). As expected, the methylation ratio is inversely correlated to the expression level.

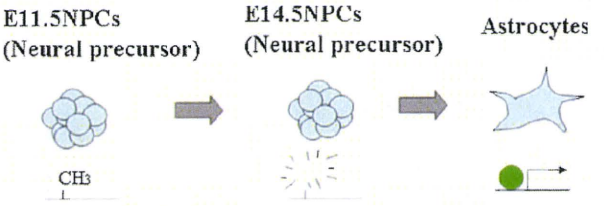

Figure 6. Model proposed for astrocyte-specific expression of the genes demethylated in E14.5 NPCs. Several astrocyte-specific genes are already demethylated in E14.5 NPCs; however, they are induced after diffentiation to astrocytes. This could be explained by astrocyte-specific transcription factors.
doi:10.1371/journal.pone.0003189.g006

Next we analyzed the average expression levels of hypermethylated and hypomethylated genes in astrocytes compared to E11.5 NPCs (Fig. 7B). Although there are some exceptions, we found the average expression levels of hypermethylated genes were low and those of hypomethylated genes were high in astrocytes. One of the reasons which could explain the existence of exceptions is the wide distribution of the probes (between −8000 to +2000 bases from the transcription start sites). Interestingly, the expression levels of hypomethylated genes were low in E14.5 NPCs compared to ones in astrocytes. This again indicates activation of expression appears after differentiation into astrocytes.

STAT and SMAD binding sites in demethylated and upregulated genes

A CpG sequence in a conserved STAT-binding site in the *Gfap* gene promoter is methylated in NPCs midgestation when astrogliogenesis does not normally commence; however, it becomes demethylated in late gestational NPCs that have gained the potential to differentiate into astrocytes [15]. Thus, the *Gfap* gene with the hypomethylated promoter can be expressed upon astrocyte differentiation induced by LIF, which activates the JAK/STAT signaling pathway [13]. Therefore, we searched for conserved STAT-binding sites in the genes hypomethylated both in E14.5 NPCs and astrocytes compared to E11.5 NPCs. To avoid omitting threshold level genes, the threshold used in E14.5 NPCs

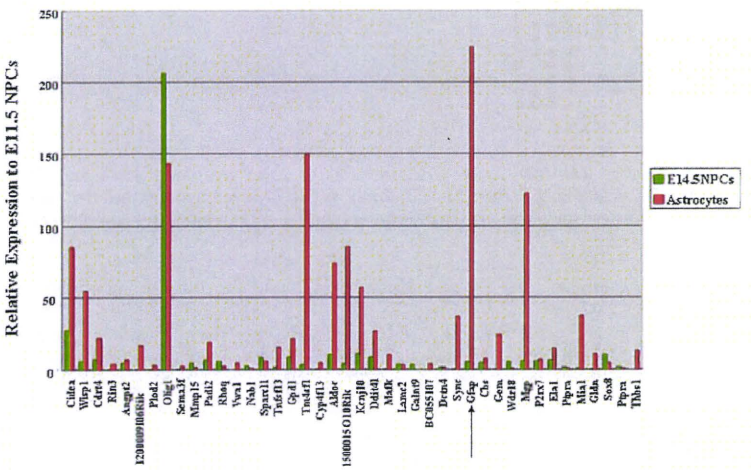

Figure 5. Expression of the genes hypomethylated both in E14.5 NPCs and astrocytes compared to E11.5 NPCs. Among hypomethylated genes, genes which showed upregulation in E14.5 NPCs or astrocytes compared to E11.5 NPCs are shown. Expression is calculated from data obtained by expression microarray analysis and presented as fold change compared to E11.5 NPCs. *Gfap* is indicated by an arrow.
doi:10.1371/journal.pone.0003189.g005

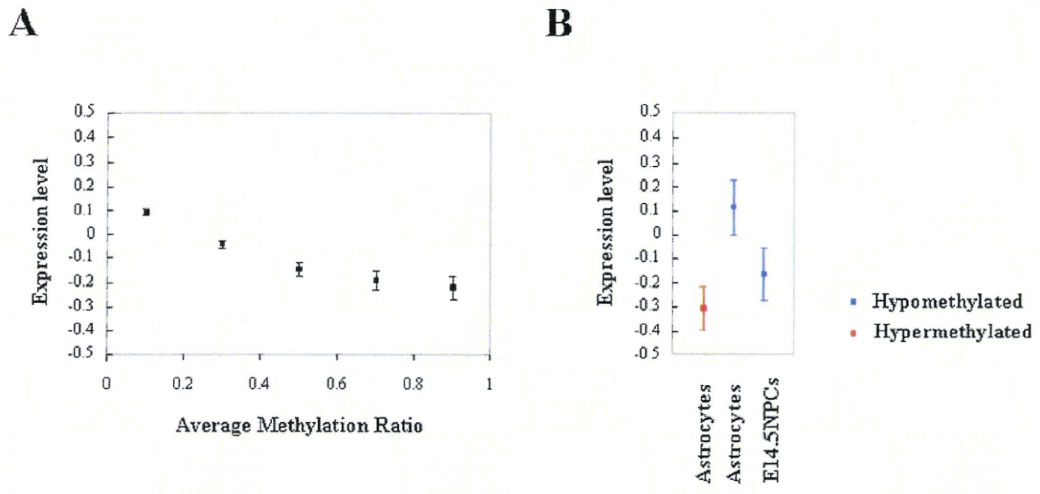

Figure 7. DNA methylation and expression. (A) All probes are grouped by their average methylation ratios and their expression levels are indicated as average±standard error of mean. Expression levels are described as normalized values in log scale. (B) Expression levels of hypermethylated (red) and hypomethylated (blue) genes in astrocytes. Expression levels are indicated as average±standard error of mean.
doi:10.1371/journal.pone.0003189.g007

was extended (D10<0.5). Among these genes, those that showed upregulation in E14.5 NPCs or astrocytes compared to E11.5 NPCs were used for analysis (Fig. 8). Sequences including 500-(basepair) bp upstream and 500-bp downstream of the probes were searched for STAT3 binding sites with the CpG sequence (TTN4-6AA, CG in any N position). Such methylation-sensitive STAT binding sites were found among these 18 genes; however, none were conserved between mice and humans except for *Gfap*, which shows hypomethylation both in E14.5 NPCs and astrocytes (Fig. 1). Although we cannot rule out the possibility that some demethylated STAT binding sites were not detected by the MIAMI method because of its target limitation, these results suggest that not all

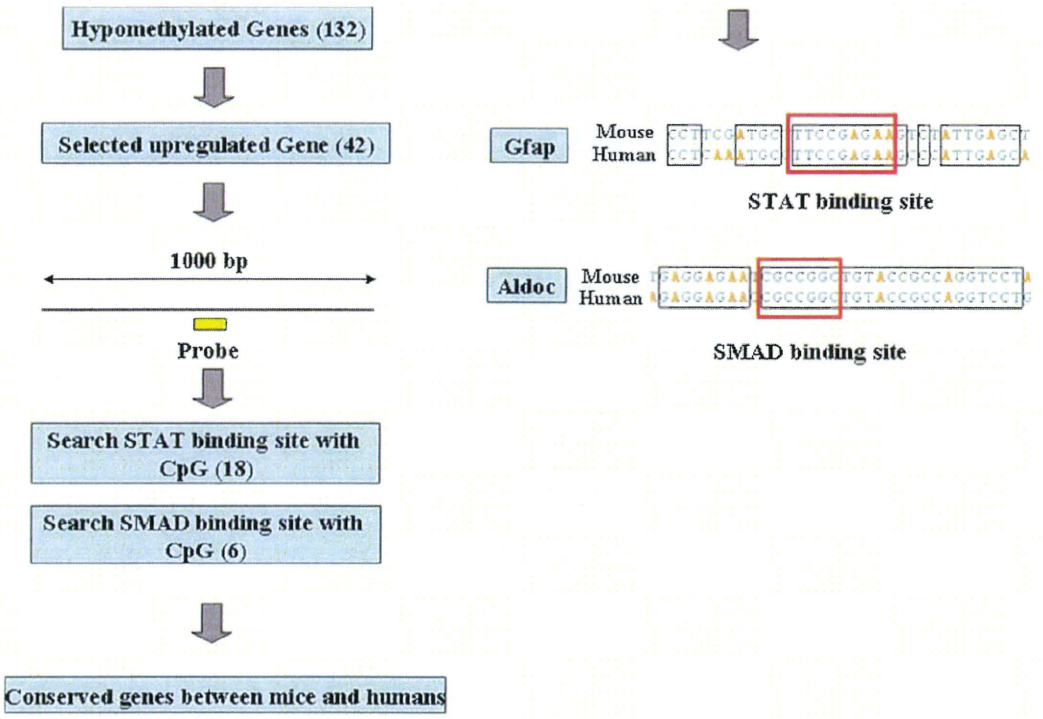

Figure 8. Screening of conserved STAT and SMAD binding sites in demethylated and upregulated genes. Schematic representation of screening of conserved STAT and SMAD binding sites in hypomethylated genes both in E14.5 NPCs and astrocytes. Numbers of genes are indicated in parentheses.
doi:10.1371/journal.pone.0003189.g008

astrocyte-specific genes are epigenetically controlled only via STAT binding site methylation.

Bone morphogenetic proteins (BMPs) also use STATs to activate the expression of astrocyte marker genes via the association between STATs and the transactivating complex composed of the MBP-activated signaling factors Smad1 and P300/CBP [33,34]. Therefore, we also searched for conserved SMADs-binding sites in the genes hypomethylated both in E14.5NPCs and astrocytes compared to E11.5 NPCs. We found methylation sensitive SMAD-binding sites in 6 genes; however, only *Aldoc* was conserved between mouse and human (Fig. 8) Bisulfite sequencing analysis of this SMAD sites reveals demethylation in E14.5 NPCs and astrocytes (Fig. 3B).

We could not find methylation-sensitive binding sites for transcription factor except for *Gfap* and *Aldoc*. Effective activation of demethylated genes in E14.5 NPCs probably requires cooperation with other transcription factors, which are activated in astrocyte differentiation.

Overrepresented genes with methylation changes

Overrepresented and underrepresented categories of genes were searched in hypomethylated and hypermethylated genes. These genes were first classified into lists using PANTHER classification categories (http://www.pantherdb.org/tools/compareToRefList-Form.jsp). Each list was then compared to the reference list using the binomial test [35] for each molecular function, biological process, or pathway term in PANTHER. Unexpectedly, there was no significant overrepresentation and underrepresentation in hypomethylated genes in E14.5 NPCs and in astrocytes ($P = 0.01$). On the other hand, biological process categories such as "mRNA transcription regulation", "developmental processes", "mRNA transcription", "neurogenesis", "ectoderm development", "nucleoside, nucleotide and nucleic acids metabolism" were overrepresented among hypermethylated genes in astrocytes ($P = 0.01$, Table 1). A molecular function category, "transcription factor", was also overrepresented among hypermethylated genes in astrocytes ($P = 0.01$, Table 1). It is reasonable that developmental genes are shut off by DNA methylation in terminally differentiated cells. A large part of developmental genes consists of the transcription factor; therefore, it is also reasonable that a category related to transcription factor such as "mRNA transcription regulation" is overrepresented in hypermethylated genes. It is interesting to know that the pathway category, "Notch signaling pathway", is overrepresented 9-fold more than expected among hypermethylated genes in astrocytes, although it is not statistically significant ($P = 0.03$). These genes include *Dll1*, *Hes1*, *Hes5*, *Hey2*, and *Ncor2* (Table 2). The Notch signaling pathway has been shown to be important in astrocyte differentiation [36]. Inactivation of developmental and transcriptional factor genes by DNA methylation is one of the important aspects of differentiation. For example, inactivation of transcription factor genes, *Oct3/4* (*Pou5f1*) and *Nanog*, by DNA methylation is important for early development [6,7]. We also found that transcription factor genes were overrepresented among methylated genes in astrocytes. Regulation by DNA methylation of transcription factor genes is an attractive model to explain development and differentiation. Usually differentiation is caused by transcription factors, which are also regulated by upstream transcription factors. So what is the most upstream regulator? One answer is that the most upstream regulator is epigenetic change.

In conclusion, we suggested in this study that many astrocyte-specific genes are demethylated in common in late-stage NPCs, enabling cells to become competent before astrocyte differentiation. This means DNA demethylation rather than methylation is a critical regulatory event in astrocyte differentiation. We also indicated that group of genes categorized as developmental and transcription factor genes are shut off by DNA methylation in terminally differentiated astrocytes.

Table 1. Overrepresented category of hypermethylated genes in astrocytes.

Biological Process	Obs/Exp	P-value
Mrna transcription regulation	3.7	1.30E-10
Developmental processes	2.8	1.35E-10
Mrna transcription	2.9	4.32E-08
Neurogenesis	3.5	4.67E-04
Endoderm development	3.2	5.93E-04
Nucleoside, nucleotide and nucleic acid metabolism	1.8	3.19E-03
Molecular Function	**Obs/Exp**	**P-value**
Transcription factor	2.9	4.29E-09

doi:10.1371/journal.pone.0003189.t001

Materials and Methods

Methylation profiling by MIAMI

The MIAMI method was performed using one microgram of genomic DNA as previously described [16,17]. The complete experimental procedure can be obtained at http://grc.dept.med.gunma-u.ac.jp/~gene/image/MIAMI%20Protocol%20V4.pdf. The microarray was the same as that used in our previous paper [17]. A brief description of the MIAMI method is as follows.

Changes in methylation were judged by using the difference in methylation-sensitive *Hpa* II cleavage and methylation-insensitive *Msp* I cleavage between samples. To detect differences in methylation-sensitive *Hpa* II cleavage, 0.5 microgram of genomic DNA was digested with 40 units of *Hpa* II overnight in a 100-microliter volume containing 33 mM Tris-acetate (pH7.9), 66 mM KOAc, 10 mM $MgOAc_2$, 0.5 mM DTT, and 0.01% BSA. The adaptor was prepared by annealing two oligonucleotides, AGCACTCTCCAGCCTCTCACCGAG and CGCTCGGTGA. After phenol extraction and ethanol precipitation, DNA was ligated to the adaptor with 60 units of E coli DNA Ligase (Takara, Japan). The first PCR was performed using 0.1 microgram of each ligation mix as a template with a primer AGCACTCTCCAGCCTCTCACCGAG using GeneTaq DNA polymerase (Nippon Gene, Japan). The reaction mixture was incubated for 5 min at 72°C and

Table 2. Hypermethylated genes in astrocytes belong to Notch signaling pathway.

Gene Symbol	Gene Name	Probe Pos
Dll1	delta-like 1	1725
Hes1	hairy and enhancer of split 1	−2503
Hes5	hairy and enhancer of split 5	−7260
Hey2	hairy/enhancer-of-split related with YRPW motif 2	−1761
Ncor2	nuclear receptor co-repressor 2	−5790

doi:10.1371/journal.pone.0003189.t002

3min at 94°C and subjected to 5 cycles of amplification consisting of 10 sec denaturation at 94°C, 30 sec annealing at 70°C, 2.5 min extension at 72°C. The final extension was lengthened to 9.5 min. Amplified DNA was digested with *Msp* I by adding 35 units of the enzyme directly to the solution. After 3-hour incubation, the digested DNA was subjected to further amplification by a second PCR. The condition was the same as in the first PCR except for the number of cycles. The optimal sub-saturation cycle number was adopted (usually 10 to 13 cycles). The PCR product was purified with a MiniElute PCR purification Kit (Qiagen, USA). To detect of differences in methylation-insensitive *Msp* I cleavage, 0.5 microgram of genomic DNA was digested with 40 units of *Msp* I overnight and subjected to the same procedure as for the amplification of unmethylated DNA fragments.

Amplified *Hpa* II-cleaved DNA fragments from two samples to be compared were labeled with Cy3 and Cy5, respectively, as described [37], and cohybridized to a microarray. All hybridization procedures except for washing were according to the manual of Agilent Technology (USA). Amplified *Msp* I-cleaved DNA fragments from two samples to be compared were labeled with Cy3 and Cy5, respectively, and cohybridized to another microarray with the same probes.

We judged spots with methylation changes using two models; one in which spots with methylation changes had different values for *Hpa* II and *Msp* I cleavage, and the other in which spots with methylation changes had a large *Hpa* II cleavage difference (more than 5) and a small *Msp* I cleavage difference (less than 2). The reproducibility of the experiment was analyzed with 885 triplicated probes on each microarray and repeated experiments.

Bisulfite genomic analysis

Bisulfite treatment of genomic DNA was performed using a CpGenome DNA modification kit (INTERGEN). Modified DNA was amplified with the primers described in Table S3. For COBRA analysis, the restriction enzymes are described in Table S3.

Expression microarray analysis

Expression microarray analysis was performed using the Agilent mouse whole genome array and the procedure provided by Agilent Technologies. A signal ratio of more than 2 with a P-value of less than 0.01 was judged as upregulated. A signal ratio of less than 0.5 with a P-value of less than 0.01 was judged as downregulated.

Animals and cell preparation

Time-pregnant ICR mice were used to prepare NPCs. The experimental protocols described below were performed according to the animal experimentation guidelines of Nara Institute of Science and Technology. NPCs were prepared from telencephalons of E11.5 and E14.5 mice and cultured as described previously [34]. Briefly, the telencephalons were triturated in Hank's balanced salt solution (HBSS) by mild pipetting with a 1-ml pipet tip (Gilson). Dissociated cells were cultured in N2-supplemented Dulbecco's Modified Eagle's Medium with F12 (GIBCO) containing 10 ng/ml basic FGF (R&D Systems) (N2/DMEM/F12/bFGF) on culture dishes (Nunc) of a chamber slide (Nunc) which had been precoated with poly-L-ornithine (Sigma) and fibronectin (Sigma). For primary astrocyte cultures, the cerebral cortices of postnatal day 1 mice were dissociated using trypsin (GIBCO), and cultured for two weeks in DMEM containing 10% fetal calf serum.

Supporting Information

Table S1 Table S1 Genome-wide profiling of DNA methylation. Hypomethylated and hypermethylated genes in E14.5 NPCs and astrocytes compared to E11.5 NPCs. Each row indicates each probe. Probes with methylation changes are indicated by color as in Fig. 1A.
Found at: doi:10.1371/journal.pone.0003189.s001 (0.06 MB XLS)

Table S2 Table S2 List of upregulated genes compared to E11.5 NPCs. Upregulated genes in E14.5 NPCs and astrocytes compared to E11.5 NPCs.
Found at: doi:10.1371/journal.pone.0003189.s002 (0.55 MB XLS)

Table S3 Table S3 List of primers and restriction enzymes used for COBRA and bisulfite sequencing analysis.
Found at: doi:10.1371/journal.pone.0003189.s003 (0.02 MB XLS)

Author Contributions

Conceived and designed the experiments: IH. Performed the experiments: IH. Analyzed the data: IH. Contributed reagents/materials/analysis tools: MN SM MK TH KN. Wrote the paper: IH KN.

References

1. Razin A, Webb C, Szyf M, Yisraeli J, Rosenthal A, et al. (1984) Variations in DNA methylation during mouse cell differentiation in vivo and in vitro. Proc Natl Acad Sci U S A 81: 2275–2279.
2. Bird A (2002) DNA methylation patterns and epigenetic memory. Genes Dev 16: 6–21.
3. Ohgane J, Aikawa J, Ogura A, Hattori N, Ogawa T, et al. (1998) Analysis of CpG islands of trophoblast giant cells by restriction landmark genomic scanning. Dev Genet 22: 132–140.
4. Song F, Smith JF, Kimura MT, Morrow AD, Matsuyama T, et al. (2005) Association of tissue-specific differentially methylated regions (TDMs) with differential gene expression. Proc Natl Acad Sci U S A 102: 3336–3341.
5. Li E, Bestor TH, Jaenisch R (1992) Targeted mutation of the DNA methyltransferase gene results in embryonic lethality. Cell 69: 915–926.
6. Hattori N, Nishino K, Ko YG, Hattori N, Ohgane J, et al. (2004) Epigenetic control of mouse Oct-4 gene expression in embryonic stem cells and trophoblast stem cells. J Biol Chem 279: 17063–17069.
7. Hattori N, Imao Y, Nishino K, Hattori N, Ohgane J, et al. (2007) Epigenetic regulation of Nanog gene in embryonic stem and trophoblast stem cells. Genes Cells 12: 387–396.
8. Niwa H, Miyazaki J, Smith AG (2000) Quantitative expression of Oct-3/4 defines differentiation, dedifferentiation or self-renewal of ES cells. Nat Genet 24: 372–376.
9. Mitsui K, Tokuzawa Y, Itoh H, Segawa K, Murakami M, et al. (2003) The homeoprotein Nanog is required for maintenance of pluripotency in mouse epiblast and ES cells. Cell 113: 631–642.
10. Chambers I, Colby D, Robertson M, Nichols J, Lee S, et al. (2003) Functional expression cloning of Nanog, a pluripotency sustaining factor in embryonic stem cells. Cell 113: 643–655.
11. Yu J, Vodyanik MA, Smuga-Otto K, Antosiewicz-Bourget J, Frane JL, et al. (2007) Science 318: 1917–1920.
12. Qian X, Shen Q, Goderie SK, He W, Capela A, et al. (2000) Timing of CNS cell generation: a programmed sequence of neuron and glial cell production from isolated murine cortical stem cells. Neuron 28: 69–80.
13. Bonni A, Sun Y, Nadal-Vicens M, Bhatt A, Frank DA, Rozovsky I, et al. (1997) Regulation of gliogenesis in the central nervous system by the JAK-STAT signaling pathway. Science 278: 477–483.
14. Rajan P, McKay RD (1998) Multiple routes to astrocytic differentiation in the CNS. J Neurosci 18: 3620–3629.
15. Takizawa T, Nakashima K, Namihira M, Ochiai W, Uemura A, et al. (2001) DNA methylation is a critical cell-intrinsic determinant of astrocyte differentiation in the fetal brain. Dev Cell 1: 749–758.
16. Hatada I, Fukasawa M, Kimura M, Morita S, Yamada K, et al. (2006) Genome-wide profiling of promoter methylation in human. Oncogene 25: 3059–3064.
17. Hatada I, Morita S, Kimura M, Horii T, Yamashita R, et al. (2008) Genome-wide demethylation during neural differentiation of P19 embryonal carcinoma cells. J Hum Genet 53: 185–191.
18. Namihira M, Nakashima K, Taga T (2004) Developmental stage dependent regulation of DNA methylation and chromatin modification in a immature astrocyte specific gene promoter. FEBS Lett 572: 184–188.

19. Walther EU, Dichgans M, Maricich SM, Romito RR, Yang F, et al. (1998) Genomic sequences of aldolase C (Zebrin II) direct lacZ expression exclusively in non-neuronal cells of transgenic mice. Proc Natl Acad Sci U S A 95: 2615–2620.
20. Higashimori H, Sontheimer H (2007) Role of Kir4.1 channels in growth control of glia. Glia 55: 1668–1679.
21. Neusch C, Papadopoulos N, Müller M, Maletzki I, Winter SM, et al. (2006) Lack of the Kir4.1 channel subunit abolishes K+ buffering properties of astrocytes in the ventral respiratory group: impact on extracellular K+ regulation. J Neurophysiol 95: 1843–1852.
22. Buono RJ, Lohoff FW, Sander T, Sperling MR, O'Connor MJ, et al. (2004) Association between variation in the human KCNJ10 potassium ion channel gene and seizure susceptibility. Epilepsy Res 58: 175–183.
23. Lenzen KP, Heils A, Lorenz S, Hempelmann A, Höfels S, et al. (2005) Supportive evidence for an allelic association of the human KCNJ10 potassium channel gene with idiopathic generalized epilepsy. Epilepsy Res 63: 113–118.
24. McKinnon PJ, Margolskee (1996) RF SC1: a marker for astrocytes in the adult rodent brain is upregulated during reactive astrocytosis. Brain Res 709: 27–36.
25. Scalabrini D, Fenoglio C, Scarpini E, De Riz M, Comi G, et al. (2007) Candidate gene analysis of SPARCL1 gene in patients with multiple sclerosis. Neurosci Lett 425: 173–176.
26. Enokido Y, Suzuki E, Iwasawa K, Namekata K, Okazawa H, et al. (2005) Cystathionine beta-synthase, a key enzyme for homocysteine metabolism, is preferentially expressed in the radial glia/astrocyte lineage of developing mouse CNS. FASEB J 19: 1854–1856.
27. Cahoy JD, Emery B, Kaushal A, Foo LC, Zamanian JL, et al. (2008) A transcriptome database for astrocytes, neurons, and oligodendrocytes: a new resource for understanding brain development and function. J Neurosci 28: 264–278.
28. Czermin B, Melfi R, McCabe D, Seitz V, Imhof A, et al. (2002) Drosophila enhancer of Zeste/ESC complexes have a histone H3 methyltransferase activity that marks chromosomal Polycomb sites. Cell 111: 185–196.
29. Müller J, Hart CM, Francis NJ, Vargas ML, Sengupta A, et al. (2002) Histone methyltransferase activity of a Drosophila Polycomb group repressor complex. Cell 111: 197–208.
30. Bernstein BE, Mikkelsen TS, Xie X, Kamal M, Huebert DJ, et al. (2006) A bivalent chromatin structure marks key developmental genes in embryonic stem cells. Cell 125: 315–326.
31. Mohn F, Weber M, Rebhan M, Roloff TC, Richter J, et al. (2008) Lineage-specific polycomb targets and de novo DNA methylation define restriction and potential of neuronal progenitors. Mol Cell 30: 755–766.
32. Mikkelsen TS, Ku M, Jaffe DB, Issac B, Lieberman E, et al. (2007) Genome-wide maps of chromatin state in pluripotent and lineage-committed cells. Nature 448: 553–560.
33. Gross RE, Mehler MF, Mabie PC, Zang Z, Santschi L, et al. (1996) Bone morphogenetic proteins promote astroglial lineage commitment by mammalian subventricular zone progenitor cells. Neuron 17: 595–606.
34. Nakashima K, Yanagisawa M, Arakawa H, Kimura N, Hisatsune T, et al. (1999) Synergistic signaling in fetal brain by STAT3-Smad1 complex bridged by p300. Science 284: 479–482.
35. Cho RJ, Campbell MJ (2000) Transcription, genomes, function. Trends Genet 16: 409–415.
36. Tanigaki K, Nogaki F, Takahashi J, Tashiro K, Kurooka H, et al. (2001) Notch1 and Notch3 instructively restrict bFGF-responsive multipotent neural progenitor cells to an astroglial fate. Neuron 29: 45–55.
37. Hatada I, Kato A, Morita S, Obata Y, Nagaoka K, et al. (2002) A microarray-based method for detecting methylated loci. J Hum Genet 47: 448–451.

Available online at www.sciencedirect.com
ScienceDirect
Neuroscience Research 61 (2008) 172–181
Neuroscience Research
www.elsevier.com/locate/neures

Significance of the deep layers of entorhinal cortex for transfer of both perirhinal and amygdala inputs to the hippocampus

Noriko Koganezawa [a], Ayaka Taguchi [a], Takashi Tominaga [b], Shinya Ohara [a], Ken-Ichiro Tsutsui [a], Menno P. Witter [c,d], Toshio Iijima [a,*]

[a] *Division of Systems Neuroscience, Tohoku University Graduate School of Life Sciences, 2-1-1 Katahira, Aoba-ku, Sendai, Miyagi 980-8577, Japan*
[b] *Department of Neurophysiology, Faculty of Pharmaceutical Sciences at Kagawa, Tokushima Bunri University, 1314-1 Shido, Sanuki, Kagawa 769-2193, Japan*
[c] *Kavli Institute for Systems Neuroscience and Centre for the Biology of Memory, Norwegian University of Science and Technology (NTNU), N-7489 Trondheim, Norway*
[d] *Department of Anatomy & Neurosciences, Institute for Clinical and Experimental Neurosciences, VU University Medical Center, Graduate School of Neurosciences, Amsterdam, 1007 MB, Amsterdam, The Netherlands*

Received 15 February 2008; accepted 21 February 2008
Available online 6 March 2008

Abstract

In the rat, a number of sensory modalities converge in the perirhinal cortex (PC). The neural pathway from the perirhinal cortex to the entorhinal cortex (EC) is considered one of the main routes into the entorhinal–hippocampal network. Evidence accumulated recently suggests that EC and PC, far from being passive relay stations, actively gate impulse traffic between neocortex and hippocampus. Using slice preparation maintaining the neurocircuit connecting PC, EC, hippocampal formation and amygdala, we investigated the associative function of PC and EC with respect to sensory and motivational stimuli and the influence of the association on the neurocircuit. In horizontal slices located ventrally to the rhinal sulcus, where we stimulated area 35 and the lateral amygdala, both inputs can be independently conveyed to the dentate gyrus. In slightly more dorsal slices where we stimulated area 36 and the lateral amygdala, the coincidence of the two inputs was needed to activate the hippocampus. This need for association of the two inputs was apparently mediated by the deep layer of EC. In all instances activation of the deep layers of EC was sufficient to activate the dentate gyrus, suggesting the relevance of the deep layers in cortico–hippocampal interactions.
© 2008 Elsevier Ireland Ltd and the Japan Neuroscience Society. All rights reserved.

Keywords: Entorhinal cortex; Perirhinal cortex; Amygdala; Hippocampus; Signal gating; Optical imaging

1. Introduction

The pathway from the perirhinal cortex (PC) to the entorhinal cortex (EC) is one of the two main entry routes for sensory information into the entorhinal–hippocampal network (Burwell and Amaral, 1998; Burwell, 2000; Burwell and Witter, 2002; Witter and Amaral, 2004). Based on our current knowledge of the network it is quite likely that various sensory modalities converge in the rat perirhinal cortex. The perirhinal cortex also interconnects with the amygdala, which plays an important role in various motivational and emotional behaviors (Ono et al., 1995; Nishijo et al., 1998). For its presumed role in declarative memory, the entorhinal–hippocampal system strongly depends on this input from the perirhinal cortex (Eichenbaum et al., 2007). Surprisingly, the projection from PC to EC features a rather unusual high level of inhibition, indicating that transfer of information only occurs when particular requirements are met by the network (de Curtis and Paré, 2004). In view of evidence that memory processing is facilitated by the emotional connotation of the information to be remembered (Cahill et al., 1995, 1996; Hamann et al., 1999; Richardson et al., 2004; Paz et al., 2006), we have previously investigated whether interactions between PC and amygdala may alter the normally inhibited transfer of information into EC. In horizontal slices of the rat obtained near the rhinal sulcus, the neural circuit connecting PC, EC, hippocampal formation, and the lateral nucleus of the amygdala (LA) is largely maintained (Iijima et al., 1994, 1996; Kajiwara et al.,

* Corresponding author. Tel.: +81 22 217 5046; fax: +81 22 217 5048.
E-mail address: t-iijima@mail.tains.tohoku.ac.jp (T. Iijima).

0168-0102/$ – see front matter © 2008 Elsevier Ireland Ltd and the Japan Neuroscience Society. All rights reserved.
doi:10.1016/j.neures.2008.02.007

2003). Using such preparations, and optical imaging with a voltage-sensitive dye, we showed that following stimulation in the superficial layers of PC, electrical activity only propagated into EC when sufficient activation occurred in the deep layers of perirhinal area 35. We observed that single stimulation of either PC or LA did not result in sufficient neural activation of the deep layers of areas 35 to provoke activity propagation into EC. However, the deep layers of area 35 were depolarized much more strongly when the two stimuli were applied simultaneously, resulting in spreading activation in EC. Our observations suggested that a functional neural basis for the association of higher-order sensory inputs and emotion-related inputs exists in PC and that transfer of sensory information to the entorhinal–hippocampal circuitry might be affected by the association of that information with incoming information from the amygdala (Kajiwara et al., 2003; Pelletier et al., 2005).

In our previous study, focus was on slices obtained dorsal to or at the rhinal sulcus, to ascertain that both areas 36 and 35 were present in the slice. Our previous findings that perirhinal area 35 was critically involved in the transfer of activity into EC are in line with anatomical data (Burwell and Amaral, 1998). Therefore, in this study, we conducted experiments in horizontal slices obtained at levels through and ventral to the rhinal sulcus such that the slices would maintain the connectivity between area 35 and the entorhinal cortex. In these preparations we observed that in some slices the neural activity evoked in the superficial layer of PC or in LA may conduct independently to the hippocampus. In this propagation of neural activity, the deep layers (V/VI) of the rhinal cortices appeared to play an important role. In some other slices, the association of the cortical input and amygdala input was essential to cause the activation of the hippocampus as seen in the previous study. In such slices, the association of these two different inputs most probably occurred in the deep layer of EC. Therefore, we conducted a whole-cell voltage clamp in the layer V neurons of EC, and found that in the deep layers of EC cells apparently receive both cortical input and amygdala input. Taken together, our findings indicate that the deep layers of EC are part of the network that integrates cortical and amygdala inputs and submits the resulting information to the dentate gyrus.

2. Materials and methods

2.1. Slice preparation and solutions

Male Wistar rats (100–160 g) were deeply anesthetized by ether and decapitated. Slices (400 μm thickness) were prepared using a vibratome (DTK-3000W, Dosaka, Japan) in ice-cold sucrose artificial cerebrospinal fluid (s-ACSF) (Moyer and Brown, 1998). The s-ACSF was composed of (in mM) 248 sucrose, 5 KCl, 1.25 NaH_2PO_4, 2 $MgSO_4$, 1 $CaCl_2$, 1 $MgCl_2$, 22 $NaHCO_3$, and 10 D-glucose, and oxygenated with a mixture of 95% O_2–5% CO_2, pH 7.4, chilled to 4 °C. The slices including the PC, EC, hippocampal formation and amygdala were cut at an angle indicated by line *h* shown in Fig. 1A. For this, the hemispheres were separated and their dorsal part removed by razor cuts parallel to line *h*, and each hemisphere was glued with its dorsal cut surface to a vibratome stage. Fig. 1B shows an example of a Nissl-stained slice cut at the level of line *h*. With the use of such slices, we investigated

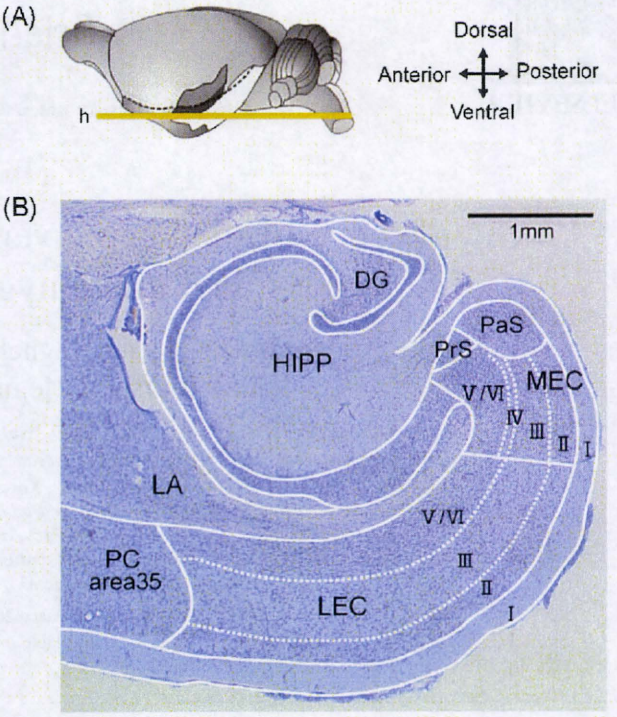

Fig. 1. Preparation of the rat brain slice. (A) Lateral view of the rat brain. Approximate orientation of the brain slice is illustrated by line *h*. (B) Nissl-stained slice. The slice includes the hippocampus (HIPP), medial and lateral entorhinal cortex (MEC, LEC), perirhinal cortex (PC), and lateral amygdaloid nucleus (LA).

propagation of neural activity following stimulation of perirhinal layers II/III and of the amygdala.

Before the start of recording, slices were submerged in the incubation chamber with standard ACSF for more than 1 h. The standard ACSF used for incubation and recording consists of (in mM) 124 NaCl, 5 KCl, 1.25 NaH_2PO_4, 2 $MgSO_4$, 2 $CaCl_2$, 22 $NaHCO_3$, and 10 D-glucose, oxygenated with a mixture of 95% O_2–5% CO_2, pH 7.4. The ACSF was maintained at room temperature (26–28 °C).

2.2. VSD (voltage-sensitive dye) imaging

The optical recording methods were similar to those reported elsewhere (Barish et al., 1996; Iijima et al., 1996; Kajiwara et al., 2003). For recording, a slice was submerged in a recording chamber mounted on a fluorescence macro zoom microscope (MVX-10, Olympus, Japan). The slice was stained in the recording chamber for 3 min with the voltage-sensitive dye RH-795 (0.5 mg/ml ACSF). The voltage-sensitive dye has excitation and emission maxima at 530 and 712 nm, respectively. Emission decreases proportionally to the changes of membrane depolarization (Grinvald et al., 1994). After the staining, extra dye was washed out with oxygenated superfusion solution and the preparation was incubated in the recording chamber for another 10–15 min before the optical measurements were performed. The magnification of the microscope was adjusted to 2.8×–3.3×, depending on the size of the objective field on the slice preparation. Illumination from a tungsten–halogen lamp (150 W) was passed through a heat filter (<10% transmittance for 700–1600 nm light). The excitation light filtered at 535 nm (±20 nm band-pass) was reflected down onto the preparations by a dichroic mirror (halfreflectance wave length of 580 nm). Epifluorescence through a long-wavelength pass filter (50% transmittance at 600 nm) was detected with a complementary metal oxide semiconductor sensor array detector (MiCAM Ultima L-camera, BrainVision, Japan; 100 μm × 100 μm pixel size, 100 × 100 pixel array). By using this optical imaging system, we acquired 512 frames at a rate of 0.5 or 1.0 ms/frame. To represent the spread of neural activity, we superimposed color-coded optical

signals on the bright-field image of the slice or the image of Nissl-stained preparation made from the brain slice subjected to the optical imaging. In this procedure, we applied a color code to the fraction of the optical signal, which exceeded the baseline noise. That is, optical signals with sizes close to the baseline noise were ignored. For reducing the baseline noise, we sometimes averaged eight identical recordings acquired with a 3 s interval. The data set was averaged in the frame memory directly. The optical signal was analyzed off-line using custom-made software or BrainVision analyzer software. Changes in membrane potential were evaluated as DF/F (F – Fo/F, where Fo is the base fluorescence level). Recordings were made in a total of 29 slices.

2.3. Electrical stimulation to the PC and the amygdala

The stimulating electrode was a tungsten bipolar electrode with a tip separation of 150 μm. Since anatomical studies indicate that layers II/III of the PC receive projections from sensory areas (Burwell and Amaral, 1998; Faulkner and Brown, 1999), we placed the stimulus electrode for the PC on layers II/III to mimic input from the sensory cortices to the PC. We placed another stimulating electrode in the lateral amygdaloid nucleus (LA) to mimic an emotional input. Initially, a single-pulse electrical stimulation of 80–100 μA for 300 μs was used. If the single stimulation was found not to be sufficient to cause measurable activation in the PC or EC in the VSD imaging, we replaced the single stimulation with a repetitive stimulation at 40 Hz for 100 ms (5 pulses at 25 ms interval), each current pulse being 80–100 μA for 300 μs.

2.4. Field potential recording

A glass recording electrode filled with normal medium (5–10 MΩ) was used. The field potential was filtered at 1 kHz low-pass filter, amplified (MEZ-8300, Nihonkoden, Japan), and digitized with the use of the optical imaging system through its external input terminal. The field potential was continuously monitored throughout the experiment, and no photodynamic effect on its amplitude was observed by the optical recording.

2.5. Slice-patch recording

Synaptic responses were recorded in the layer V neurons of LEC with a whole-cell voltage clamp *in vitro* when either PC or LA, or both PC and LA were stimulated. We made patch clamp recordings on pyramidal-like neurons, although we did not identify the species of neurons precisely in this study. For slice patch recordings each slice was transferred onto a fine-mesh membrane filter (Omni Pore membrane filter, JHWP01300, Millipore, USA) held in place by a thin plexiglas ring (inner diameter, 11 mm; outer diameter, 15 mm; thickness 1–2 mm; Tominaga et al., 2000). Slices placed in the plexiglas ring were transferred to a moist holding chamber continuously supplied with a moistened mixture of the 95% O_2, 5% CO_2 gas mixture. After 1 h of incubation in this chamber, a slice on the holding ring was transferred onto an experimental chamber placed on a fixed stage and subjected to the experiments. Patch-clamp recordings in the whole-cell mode were made using a patch-clamp amplifier with a capacitive headstage (Axoclamp 200B, Axon Instruments, USA) using pipettes (3–5 MΩ) of borosilicate glass (Sutter Instruments, USA) pulled using a P-97 Flaming–Brown pipette puller (Sutter Instruments, USA). Whole-cell recordings were low-pass-filtered at 3 kHz and digitized at 10 kHz. Data were digitized with a digitizer (Digidata 1342, Axon Instruments, USA) and fed into a computer for off-line analysis (Next Computer) using software AxoClamp 9.0 (Axon Instruments, USA). Electrical stimulations were applied by constant current pulses (SS-202J with SEN-7203, Nihonkoden, Japan) through a bipolar tungsten electrode placed in layer II/III of PC and LA. Stimulation was given for 300 μs and the intensity was varied in the range of 80–100 μA to obtain EPSCs. Neurons were visualized by oblique illumination with the aid of the contrast enhancement of a CCD-camera (C2741, Hamamatsu photonics, Japan) mounted on an upright microscope (Axioskop 2FS, Ziess, Oberkochen, Germany). In voltage-clamp mode, a test membrane potential step (−10 mV) was always applied prior to electrical stimulation, and traces with series resistance lower than 20 MΩ were accepted. The pipette solution consisted of, in mM: 130 Cs-$MeSO_3$, 10 Hepes, 4 $MgCl_2$, 4 NaATP, 0.4 NaGTP, 10 Na-Phosphocreatine, 10 EGTA; pH was adjusted to 7.2.

2.6. Drugs

The entorhinal cortex has been reported to harbor many more cells containing the calcium-binding protein parvalbumin than is the case for the PC. Since it has been well established in these areas that parvalbumine colocalize for 100% with GABA, it is likely that, in the EC, more GABA-containing cells will be present compared with the PC (Burwell et al., 1995; Miettinen et al., 1996; Wouterlood et al., 2004). To investigate the spatiotemporal distribution of excitatory activities between the PC and the entorhinal–hippocampal circuit, synaptic inhibition was partly suppressed by applying a low concentration of the GABAA antagonist bicuculline (1–2 μM) ((−)-bicuculline methiodide, Sigma–Aldrich Co., USA) in the recording solution as reported previously (Kajiwara et al., 2003). Under such conditions, the optical imaging with voltage-sensitive dye has already measured spread of neural activity in the entorhinal–hippocampal network elicited by electrical stimulation to LEC in rat brain slices without inducing spontaneous paroxysmal activities (Iijima et al., 1994, 1996).

2.7. Histology

The brain slices of 400 μm thickness were fixed with 4% paraformaldehyde for more than 1 week. Subsequently, the slices were stored in PBS with 30% sucrose for more than 10 h and cut at 50 μm thickness with the use of a freezing microtome (SM-2000R, Leica Microsystems, Germany). Sections were Nissl-stained in 0.25% thionin solution. Fig. 1B shows the histological result. The areas of the perirhinal and entorhinal cortices were delineated on the bases of cytoarchitectural criteria (Burwell et al., 1995; Insausti et al., 1997). In the perirhinal cortex, we differentiated between areas 35 and 36 and for the entorhinal cortex a division into lateral entorhinal cortex (LEC) and medial entorhinal cortex (MEC) was used. By comparing these histological data with the optical imaging data, we could identify the region in which neural propagation occurred. In some analyses we superimposed the spatio-temporal activation pattern detected with VSD imaging onto the Nissl-stained preparation obtained from that same slice as shown in Fig. 2.

3. Results

3.1. Propagation of neural activity evoked in the superficial layer of the PC or in the amygdala

In this study horizontal slices were obtained through the ventral part of the rat brain, below and apart from the rhinal sulcus for at least 300 μm (Fig. 1A). Fig. 1B shows a Nissl-stained example of the slices used in this study. The slice preparations contained the PC, EC, hippocampal formation, and amygdala. In all our slices we noticed that both LEC and MEC were present, and could be easily distinguished. Since we aimed for slices directly ventral to or including the ventral bank of the rhinal sulcus, area 36 was expected not to be present. In some of our slices, however, area 36 was still present, most likely due to a slightly different cutting angle, and in those instances our stimulation site quite generally was in area 36. Note that during the course of the imaging experiments, it was hard to confirm the structure of the perirhinal cortex. So, we examined the site of stimulation afterwards, based on the cytoarchitecture as revealed by the Nissl-stained preparation of the slice subjected to the VSD imaging.

First we investigated propagation of neural activity following stimulation of layers II/III of PC (hereafter a PC stimulation) which mimics a sensory input, and stimulation of the lateral amygdala which mimics an emotional input (hereafter an LA stimulation). In Fig. 2A and D, the spatio-temporal propagation pattern of neural activity evoked by the PC stimulation (Fig. 2A)

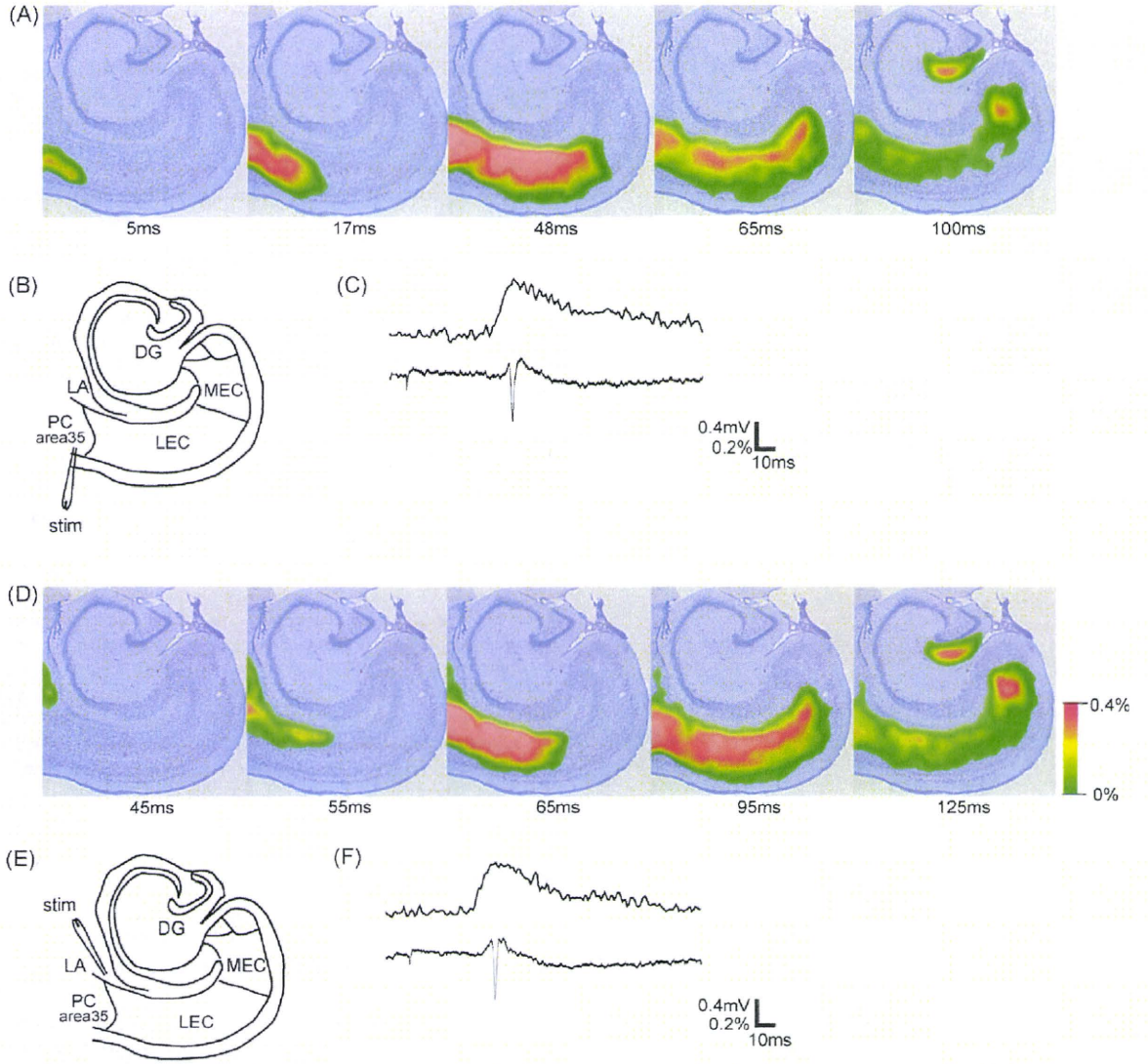

Fig. 2. (A, D) Propagation of the evoked activity in the superficial layer of PC (A) and in LA (D). To represent the spread of neural activity, the color-coded optical signal was superimposed on the image of Nissl-stained preparation made from the brain slice subjected to the optical imaging. (B, E) Arrangement of the stimulating electrode. (C, F) Simultaneous recordings of an optical signal (upper trace) and a field potential (lower trace) in the dentate gyrus.

or by the LA stimulation (Fig. 2D) is shown respectively. A single pulse stimulation (Section 2) was used in each recording. In these figures we superimposed the propagation pattern of neural activity obtained with VSD imaging on the image of Nissl-stained section obtained from the brain slice which was subjected to the VSD imaging experiment. The simultaneous recordings of the optical signal change and the field potential change in the dentate gyrus of the hippocampal formation (DG in Fig. 2B and E) associated with the PC stimulation or LA stimulation are shown in Fig. 2C and F, respectively.

When a single stimulation was applied to the superficial layer of the PC at 0 ms in Fig. 2A, evoked activity spread at 17 ms to the superficial layer of EC beyond the PC/EC border, which seems to be consistent with the anatomical observation that the perirhinal projection to the entorhinal cortex terminates mainly in layers II and III (Burwell and Amaral, 1998). In all slices subjected to the VSD imaging (29/29), we did not observe any amygdala activation following stimulation of superficial layer of entorhinal cortex. After 17 ms, the domain of the activity appeared to move to the deep layer of the EC (48 ms). The activity subsequently spread medially in the deep layers of EC (65 ms). It is reported that inhibition, mediated by GABA, is more pronounced in layer II than in layer V (Berretta and Jones, 1996; Wood and Jones, 1998; Woodhall et al., 2005). The fundamental differences of the inhibitory systems in deep and superficial layers of the EC may thus cause the spread of neural activity to occur mainly in the deep layers of the EC. The neural activity evoked in the superficial layer of the PC was finally propagated the DG (Fig. 2A, 100 ms). The activation of a part of the deep layers of the EC, near the border of LEC and MEC as shown in the pattern of 100 ms, always preceded the activation of the DG. The field potential recording in Fig. 2B clearly shows that not only population EPSPs but also population spikes were generated in the DG.

The LA stimulation was also applied in the same slice. The evoked neural activity in LA came out from the amygdala to the deep layer of PC, then spread medially in the deep layer of PC and EC (Fig. 2D, 45, 55 ms), and finally reached to the DG. Simultaneous recording in Fig. 2F also shows that the excitation caused in DG was strong enough to generate action potentials. If we compare the propagation patterns in Fig. 2A and D, each propagation pattern appeared to be quite similar. Twenty nine horizontal slices, taken at the ventral level as specified, were subjected to the VSD imaging study for analyzing the propagation of neural activity. The propagation patterns as shown in Fig. 2 were observed in 12/29 slices. In all 12 slices, histological assessment of the slice afterwards revealed that the site of stimulation was in area 35.

3.2. Associative stimuli to the PC and the amygdala

In some other slices used in this experiments (7/29), only co-activation of PC and LA, with individual stimuli being applied within a certain critical interval, resulted in the activation of DG (Fig. 3C), and independent stimulation to PC or LA failed to activate DG. In all 7 cases, the stimulation site was in area 36. The observations were quite similar to those reported previously (Kajiwara et al., 2003). In Fig. 3, a typical example is shown. In this particular slice, a single stimulation was applied to the superficial layers of PC and a repetitive stimulation (5 stimuli at 25 ms interval: Section 2) was applied to LA (Fig. 3D). The evoked activity in the superficial layers of PC expanded beyond the area of initial excitation in PC, and the excitation was propagated to almost the whole extent of LEC at 80 ms after stimulation (Fig. 3A). However no activation was observed in MEC and in the hippocampal formation in the recordings after this period. Similarly, the activation of LA, which was followed by the activation of PC and successive activation of LEC, also failed to spread beyond the border of LEC and MEC (Fig. 3B). However, when a single stimulation was applied to the superficial layer of PC 60 ms after the start of the application of a repetitive stimulation to LA, the excitation spread beyond the border of LEC and MEC and finally DG was activated (Fig. 3C).

The critical interval of the delivery of two stimuli had a variation in each experiment, although the optimal interval which resulted in the maximum response in DG was constant in each slice preparation. In 10/29 slices, no activation was observed in DG, even when PC and LA were co-activated.

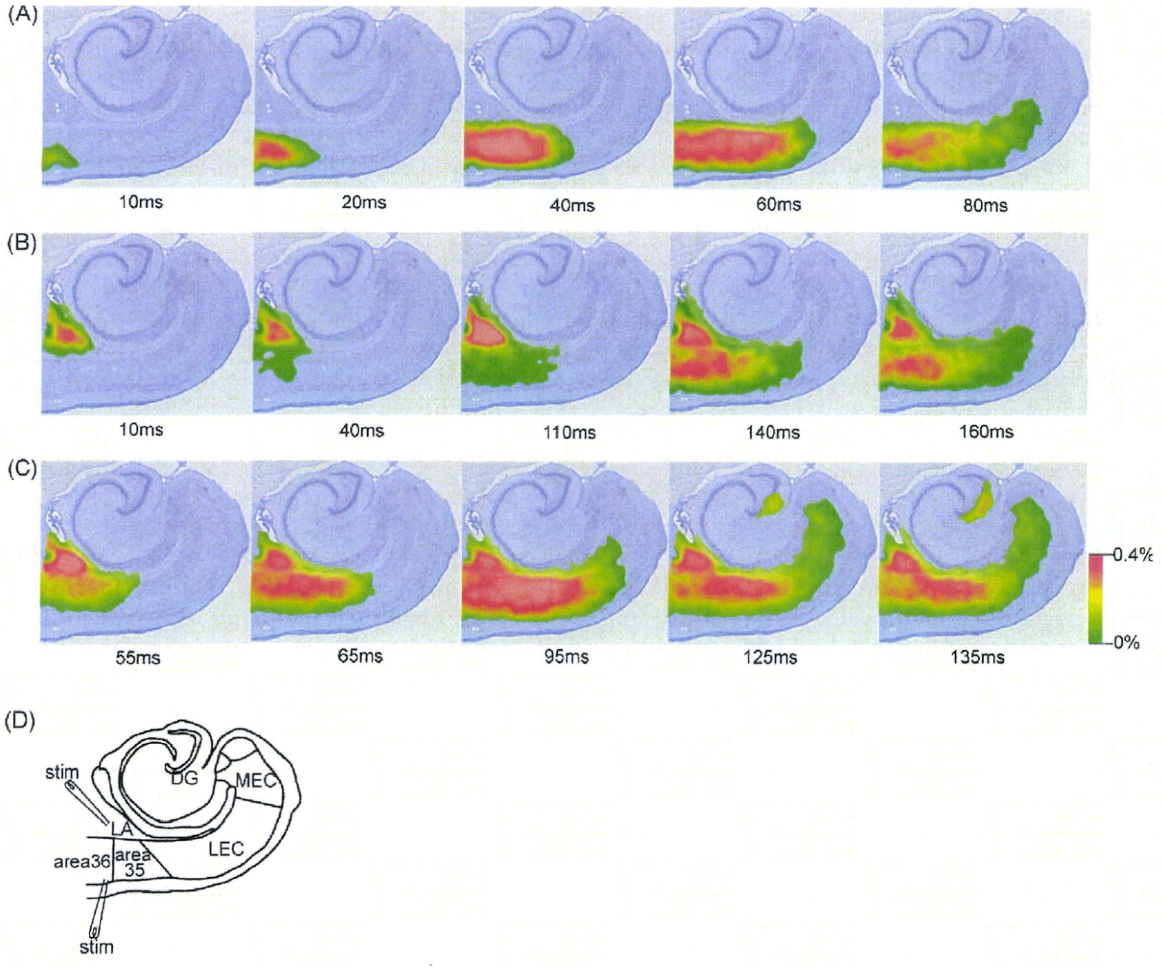

Fig. 3. Propagation of neural activity in the slice preparation. The neural activity was evoked by the stimulation of the superficial layer of PC (A) or of LA (B), or co-stimulation of LA and PC (C). (D) Arrangement of the stimulating electrodes.

3.3. Interaction of the cortical pathway and amygdala pathway

These results thus indicate that the transfer of information from amygdala and perirhinal cortex may occur in an independent as well as dependent manner and that the outcome most likely depends on the dorsal to ventral level of the slice, implying a different efficacy for perirhinal areas 35 and 36, as well as for more dorsal and ventral domains of the lateral nucleus of the amygdala. This does not exclude the possibility that even in the situation that the two inputs do result in dentate activation independently, they do interact when applied simultaneously. That such interaction may take place is quite likely in view of the consistent observation that activation in the dentate gyrus, when taking place, was always preceded by activity increases in the deep layers of the entorhinal cortex, irrespective of the stimulation protocol that was used. This thus suggests that the deep layers of the entorhinal cortex may hold a relevant portion of the neural circuitry for both inputs to reach the dentate gyrus. The potential role of the deep layers was therefore further studied.

If the two neuronal pathways are absolutely independent, individual neural activations caused in the rhinal cortices by PC stimulation or by LA stimulation are expected to be independent as well and the changes in signal should reflect that. In VSD imaging, each pixel of an image sensor records the sum of the membrane potential changes of every membranous structure projected onto the pixel. Thus, fluctuations of the optical signal from baseline represent the sum of membrane potential changes (Grinvald et al., 1982). Then we can compare the size of the evoked neural events, or more correctly the size of total membrane potential changes associated with neural activity in the different stimulation protocols, assuming that in all instances the contribution of glial cells to the signal will be constant (Otsu et al., 2000). To test whether the signal changes evoked by stimulations of the two pathways are independent or not, we measured the size of neural events in the deep layer of the rhinal cortices when the activities are evoked by only PC stimulation, by LA stimulation only, and by the co-stimulation of PC and LA (Fig. 4A and B). Then we compared the mathematical sum of the measured responses to the responses associated with the co-stimulation of PC and LA (Fig. 4C). We hypothesized that if the cortical and amygdala pathways are absolutely independent, the mathematical sum of the size of neural event associated with only PC stimulation and that associated with only LA stimulation would be almost equal to the size of neural event associated with the co-stimulation of PC and LA. As shown in columns 1–12 of Fig. 4C (corresponds to number of sample points 1–12 as seen in Fig. 4A), this is not the case. That is, a non-linearity is seen over all of the columns. In columns 1–6, the sum of the responses associated with the two single stimulations exceeds that associated with the co-stimulation of PC and LA. In contrast, in columns 7–10, the situation is totally reversed. Here, the magnitude of the measured signal changes associated with co-stimulation of PC and LA exceeds the sum of the individually evoked responses. This means that the simultaneous stimulation of the two inputs strengthened the overall neural excitation in these regions. This effect may further cause the additional excitations in the regions of 11 and 12, although no excitability was measured in these areas following independent stimulations of PC or of LA (Fig. 4B, traces in 11 and 12). The associative effect was most prominent in the deep layers, compared to the effect observed in the superficial layers using the same procedure (data not shown). We have performed the same analysis as shown in Fig. 4 on seven slices, and obtained similar result in each slice.

3.4. Integration of cortical and amygdala inputs

The results shown in Fig. 4 strongly suggest that the cortical and amygdala pathways into the entorhinal–hippocampal system share at least parts of their neurocircuits, mediating integration of the two inputs. Such integration appears to strengthen the overall neural response, resulting eventually in the transfer of neural activity to the dentate gyrus. The sampling points of the data represented in columns 7–10 (Fig. 4) are in the deep layers of the medial part of LEC and the adjacent part of MEC. It has been reported that neurons of LA project, among others, to layer V neurons in LEC (Krettek and Price, 1977; Pikkarainen et al., 1999; Rosenkranz and Johnston, 2007). When combining all these data, it is most likely that the integration of the two inputs takes place in the deep layers of LEC, although it cannot be excluded that the perirhinal areas 35 and 36 may mediate integration as well.

To examine the possibility that the integration is mediated by the neurons in the deep layers of LEC, we performed patch-clamp recordings in visually identified layer V neurons in the medial part of LEC. In individual experiments, we tried to record the synaptic current from the same neuron while either PC or LA, or both were stimulated. We made whole cell recordings in 16 cells and found that all of them respond to each stimulation, indicating that they receive both cortical and amygdala inputs. In Fig. 5, a typical result is shown. In the upper panel, ten consecutive recordings are superimposed. In A and B, only PC or LA was stimulated respectively, while PC and LA were co-stimulated in C. In this particular case, the cell sometimes failed to respond to LA stimulation. In other cells, such failures were also observed following PC stimulations. However, every neuron in the deep layer of the entorhinal cortex which was subjected to the patch-clamp recordings did not fail to respond to the associative stimulation at all. This appears to be the effect of integration of the two inputs which is expected to strengthen the synaptic connectivity. Where the integration does occur remains to be clarified. In the lower panel a typical EPSC was selected from the EPSCs shown in the upper panel. The amplitudes of the averaged as well as of single EPSC for both the single PC and LA stimulation are not significantly different from those seen after co-stimulation of both inputs. The EPSCs obtained from other neurons had a similar nature as those shown in Fig. 5.These findings indicate that single cells are not likely to receive both inputs but the fact that all these cells responded to both inputs is taken to support the concept that the network comprising neurons in layer V of LEC is integrating these two inputs as to provide active transfer to DG.